

Structural flexibility of the heme cavity in the cold-adapted truncated hemoglobin from the Antarctic marine bacterium *Pseudoalteromas haloplanktis* TAC125

Journal:	<i>FEBS Journal</i>
Manuscript ID:	FJ-15-0075
Manuscript Type:	Regular Paper
Subdiscipline:	Structural biology
Date Submitted by the Author:	30-Jan-2015
Complete List of Authors:	<p>Giordano, Daniela; National Research Council (CNR), Institute of BioSciences and BioResources (IBBR)</p> <p>Pesce, Alessandra; University of Genova, Department of Physics</p> <p>Boechi, Leonardo; University of Buenos Aires, Dept. of Inorganic Chemistry, Analytical Chemistry & Physics</p> <p>Bustamante, Juan Pablo; University of Buenos Aires, Dept. of Inorganic Chemistry, Analytical Chemistry & Physics</p> <p>Caldelli, Elena; University of Firenze, Department of Chemistry "Ugo Schiff"</p> <p>Howes, Barry D.; University of Firenze, Department of Chemistry "Ugo Schiff"</p> <p>Riccio, Alessia; National Research Council, Institute of Biosciences and BioResources</p> <p>di Prisco, Guido; National Research Council (CNR), Institute of BioSciences and BioResources (IBBR)</p> <p>Marco, Nardini; University of Milan, Dept. of Biosciences</p> <p>Estrin, Dario; University of Buenos Aires, Dept. of Inorganic Chemistry, Analytical Chemistry & Physics</p> <p>Smulevich, Giulietta; University of Firenze, Dept. of Chemistry</p> <p>Bolognesi, Martino; University of Milan, Dept. of Biomolecular Sciences & Biotechnology; University of Milano, CNR-Institute of Biophysics and CIMAINA</p> <p>Verde, Cinzia; National Research Council (CNR), Institute of BioSciences and BioResources (IBBR)); Roma 3 University, Department of Biology</p>
Key Words:	Adaptation, Bacterial hemoglobin, Resonance Raman, X-ray structure, Molecular dynamics

Structural flexibility of the heme cavity in the cold-adapted truncated hemoglobin from the Antarctic marine bacterium *Pseudoalteromonas haloplanktis* TAC125

Daniela Giordano^{1*}, Alessandra Pesce^{2*}, Leonardo Boechi³, Juan Pablo Bustamante³, Elena Caldelli⁴, Barry D. Howes⁴, Alessia Riccio¹, Guido di Prisco¹, Marco Nardini⁵, Dario Estrin³, Giulietta Smulevich^{4,§}, Martino Bolognesi^{5,6,§}, Cinzia Verde^{1,7,§}

¹Institute of Biosciences and BioResources, National Research Council, Via Pietro Castellino 111, I-80131 Napoli, Italy; ²Department of Physics, University of Genova, Via Dodecaneso 33, I-16146 Genova, Italy; ³Departamento de Química Inorgánica, Analítica y Química Física, Universidad de Buenos Aires, Ciudad Universitaria, C1428EGA, Argentina; ⁴Department of Chemistry “Ugo Schiff”, University of Firenze, Via della Lastruccia 3-13, I-50019 Sesto Fiorentino (Fi), Italy; ⁵Department of Biosciences, University of Milano, Via Celoria, 26, I-20133 Milano, Italy; ⁶CNR-Institute of Biophysics and CIMAINA, University of Milano, I-20133 Milano, Italy; ⁷Roma 3 University, Department of Biology, Viale Marconi 446, I-00146 Roma, Italy.

*These authors contributed equally to this work

§Corresponding authors:

G. Smulevich, Department of Chemistry “Ugo Schiff”, University of Firenze, Via della Lastruccia 3-13, 50019 Sesto Fiorentino (Fi), Italy; Tel. +39 0554573083; Fax +39 0554573077; e-mail: giulietta.smulevich@unifi.it;

M. Bolognesi, Department of Biosciences, University of Milano, Via Celoria, 26, 20133 Milano (Italy); Tel. +39 0250314893; Fax +39 0250314895; e-mail: martino.bolognesi@unimi.it

C. Verde, Institute of Biosciences and BioResources, National Research Council, Via Pietro Castellino 111, 80131 Napoli, Italy; Tel./Fax +39 0816132710; e-mail: cinzia.verde@ibbr.cnr.it.

Running title: Heme-cavity flexibility in an Antarctic bacterial hemoglobin

Abbreviations

Truncated hemoglobin, TrHb; TrHbII from *Pseudoalteromonas haloplanktis* TAC125, *Ph*-2/2HbO; myoglobin, Mb; flavohemoglobins Fhb; single-domain globin, SDHb; TrHbII from *Mycobacterium tuberculosis*, *Mt*-2/2HbO; TrHbII from *Thermobifida fusca*, *Tf*-2/2HbO; TrHbII from *Bacillus subtilis*, *Bs*-2/2HbO; TrHbII from *Geobacillus stearothermophilus*, *Gs*-2/2HbO; TrHbII from *Agrobacterium tumefaciens*, *At*-2/2HbO; TrHbII from *Arabidopsis thaliana*, *Ath*-2/2HbO; *Pseudoalteromonas haloplanktis* TAC125, *Ph*TAC125; Resonance Raman spectroscopy, RR; Electron Paramagnetic Resonance spectroscopy, EPR; Molecular

1
2 Dynamics, MD; Quantum Mechanics, QM; Density Functional Theory, DFT; Perdew-Burke-
3
4 Ernzerhof, PBE; High-Spin, HS; Low-Spin, LS; Root Mean Square Deviation, RMSD; Implicit
5
6 Ligand Sampling, ILS; hexa-coordinated heme state, 6c; penta-coordinated heme state, 5c;
7
8
9 Horseradish Peroxidase Isoenzyme C, HRPC.

10 11 12 13 **Database**

14
15
16 Structural data have been submitted to the Protein Data Bank under accession numbers 4UUR
17
18 and R4UURSF.

19 20 21 22 23 **Keywords**

24
25 Adaptation, Bacterial hemoglobin, Resonance Raman, X-ray structure, Molecular dynamics
26
27
28
29
30
31
32
33
34
35
36
37
38
39
40
41
42
43
44
45
46
47
48
49
50
51
52
53
54
55
56
57
58
59
60

Abstract

Truncated hemoglobins build one of the three branches of the globin protein superfamily. They display a characteristic two-on-two α -helical sandwich fold and are clustered into three groups (I, II, and III) based on distinct structural features. Truncated hemoglobins are present in eubacteria, cyanobacteria, protozoa and plants. Here we present a structural, spectroscopic and molecular dynamics characterization of a group-II truncated hemoglobin, encoded by the *PSHAa0030* gene from *Pseudoalteromonas haloplanktis* TAC125 (*Ph-2/2HbO*), a cold-adapted Antarctic marine bacterium hosting one flavohemoglobin and three distinct truncated hemoglobins. *Ph-2/2HbO* aquo-met crystal structure (at 2.21 Å resolution) shows typical features of group-II truncated hemoglobins, namely the two-on-two α -helical sandwich fold, a helix Φ preceding the proximal helix F, and a heme distal-site hydrogen bonded network that includes water molecules and several distal-site residues, among which His(58)CD1. Analysis of *Ph-2/2HbO* by electron paramagnetic resonance, resonance Raman and electronic absorption spectra, under varied solution conditions, shows that *Ph-2/2HbO* can access diverse heme ligation states. Among these, detection of a low-spin heme hexa-coordinated species suggests that residue Tyr(42)B10 can undergo large conformational changes in order to act as the sixth heme-Fe ligand. Altogether, the results show that *Ph-2/2HbO* maintains the general structural features of group-II truncated hemoglobins, but displays enhanced conformational flexibility in the proximity of the heme cavity, a property likely related to the functional challenges, such as low temperature, high O₂ concentration and low kinetic energy of molecules, experienced by organisms living in the Antarctic environment.

Introduction

The most recent bioinformatics search for globin-like sequences identified putative globins in more than one half of the 2200 sequenced bacterial genomes. A comprehensive nomenclature, including prokaryotic and eukaryotic globins, assigns globins to three distinct families: (i) the myoglobin (Mb)-like family displaying the classical three-on-three (3/3) α -helical sandwich fold, and including flavohemoglobins (FHbs) and single-domain globins (SDHbs); (ii) the sensor globin family; and (iii) the truncated hemoglobin (TrHb) family, that displays the two-on-two (2/2) α -helical sandwich fold [1]. Members of the TrHb family have been found in eubacteria, cyanobacteria, protozoa and plants, but not in animals [2]. On the basis of phylogenetic analyses, the TrHb family can be further divided into three distinct sub-families: TrHbI (or N), TrHbII (or O), and TrHbIII (or P); specific structural features related to sequence motifs, heme cavity, helices in their folds, and protein matrix tunnel(s) distinguish each group [2,3].

Several sequence and 3D structure analyses of the TrHbII group have been reported. To date, six TrHbII crystal structures have been described, of *Mycobacterium tuberculosis* (*Mt*-2/2HbO, [4]), *Thermobifida fusca* (*Tf*-2/2HbO, [5]), *Bacillus subtilis* (*Bs*-2/2HbO, [6]), *Geobacillus stearothermophilus* (*Gs*-2/2HbO, [7]), *Agrobacterium tumefaciens* (*At*-2/2HbO, [8]), and of the first plant TrHb from *Arabidopsis thaliana* (*Ath*-2/2HbO, also called AtGLB3 or AHb3, [9]). Besides sequence signatures that translate into tertiary structure features, the most distinctive feature of TrHbIIs is the presence of specific heme distal residues at the B10, CD1, E7, E11, and G8 topological sites, which are implied in modulation of heme ligand binding [2,3].

TrHbs have also been identified in the cold-adapted Antarctic marine bacterium *Pseudoalteromonas haloplanktis* TAC125 (*Ph*TAC125): one TrHbI (encoded by the *PSHAa0458* gene), and two distinct TrHbIIs (encoded by *PSHAa0030* and *PSHAa2217*) [10]. Amino-acid sequence identity between the two TrHbIIs is only 24%, suggesting that these

1
2 proteins may play different function(s) in the bacterial metabolism. Moreover, *PhTAC125*
3
4 hosts one FHb, annotated as *PSHAa2880* [10]. To our knowledge, *PhTAC125* provides the first
5
6 example of coexistence of genes encoding one FHb and three TrHbs [11]. The presence of
7
8 multiple globin genes supports the idea of their involvement in a protection mechanism against
9
10 oxidative and nitrosative stress in a cold and O₂-rich environment such as Antarctica [12].
11
12

13
14 In particular, TrHbII encoded by the *PSHAa0030* gene, named *Ph-2/2HbO*, has been
15
16 thoroughly investigated from the biochemical and functional viewpoints [10,12-16]. The
17
18 inactivation of the *PSHAa0030* gene encoding *Ph-2/2HbO* makes the mutant bacterial strain
19
20 sensitive to high O₂ levels, hydrogen peroxide, and nitrosating agents [12]. In contrast,
21
22 overexpression of the *PSHAa0030* gene in a mutant *Escherichia coli* defective of FHb and
23
24 hypersensitive to nitrosative stress indicates that *Ph-2/2HbO* protects growth and cellular
25
26 respiration of the heterologous host against the toxic effect of NO-donors. Moreover, the ferric
27
28 form of *Ph-2/2HbO* was shown to catalyse peroxynitrite isomerisation *in vitro*, confirming its
29
30 potential role in reactive nitrogen species scavenging [16].
31
32
33
34

35
36 Here we report a comprehensive study of *Ph-2/2HbO*, combining its crystal structure
37
38 (solved at 2.21 Å resolution) with a spectroscopic analysis based on Resonance Raman (RR)
39
40 and Electron Paramagnetic Resonance (EPR), and complemented by molecular dynamic (MD)
41
42 simulations. The RR solution data highlight spin population differences between the solution
43
44 and the crystalline states, suggesting a flexible architecture of the protein structure in proximity
45
46 of the heme cavity, not previously observed in other TrHbs. The structural and dynamic
47
48 features relevant for determining the ligand-binding properties and flexibility of *Ph-2/2HbO* are
49
50 considered.
51
52
53
54
55

56 **Results**

57 *Structure of Ph-2/2HbO*

58
59
60

1
2 The 3D structure of aquo-met *Ph-2/2HbO* (devoid of the first nineteen residues, see
3
4 Materials and Methods) was solved using crystals belonging to the orthorhombic space group
5
6 $P2_12_12_1$, hosting two protein chains (A and B) per asymmetric unit (**PDB ID: 4UUR** and
7
8 **R4UURSF**, respectively). The structure was refined at 2.21 Å resolution to a final R-factor and
9
10 R-free values of 18.3% and 24.6%, respectively, with ideal stereochemical parameters (Table
11
12 1). Conformational disorder affects the N-terminal 20-21 residues of both *Ph-2/2HbO* chains,
13
14 whose electron density was lost to the solvent.
15
16

17
18 Superposition of 124 C_α atoms of the two independent chains yields a Root Mean Square
19
20 Deviation (RMSD) of 0.38 Å. The results discussed below apply equally to both the A and B
21
22 chains unless otherwise stated. Analysis of the *Ph-2/2HbO* dimeric assembly, by means of the
23
24 program PISA (http://www.ebi.ac.uk/msd-srv/prot_int/cgi-bin/piserver) [18], did not highlight
25
26 a significant association interface between the A and B chains in the crystal asymmetric unit
27
28 that could justify a stable quaternary assembly (Fig. S1). This finding is in agreement with the
29
30 results of size-exclusion chromatography experiments that identified the protein as a monomer
31
32 in solution [10].
33
34
35
36
37
38
39

40 *Structural comparison with other TrHbIIs*

41
42 The *Ph-2/2HbO* tertiary structure displays the typical features of the α -helical 2/2Hb-fold
43
44 [2,3,19], with some structural modifications that are specific for TrHbIIs, such as an additional
45
46 α -helix (Φ helix, residues 82-87 in *Ph-2/2HbO*) located between helices E and F (Figs. 1 and
47
48 2) [4]. Structural superposition of *Ph-2/2HbO* on *At-2/2HbO*, *Mt-2/2HbO*, *Tf-2/2HbO*, *Bs-*
49
50 *2/2HbO*, *Gs-2/2HbO* and *Ath-2/2HbO* yields RMSD values in the 0.9-1.2 Å range, the best
51
52 match being with *At-2/2HbO*. The main differences relative to other TrHbIIs (taking *Mt-*
53
54 *2/2HbO* as reference, see alignment in Fig. 2) are located in the N-terminal region (where full-
55
56 length *Ph-2/2HbO* hosts a sequence extension of nineteen residues, proteolytically cleaved
57
58 during protein purification), in the BC (three-residue insertion in *Ph-2/2HbO*), CE (one-residue
59
60

1
2 deletion in *Ph-2/2HbO*) and GH (three-residue deletion in *Ph-2/2HbO*) loops, and in the C-
3
4 terminal region. The two Gly-Gly motifs present at the C-terminal end of helices A and E,
5
6 typical of TrHbI and TrHbII, are conserved in *Ph-2/2HbO*, helping stabilization of the short
7
8 helix A in a conformation locked onto helices B and E (Fig. 1).
9

10
11 Analysis of the crystal structure reveals that in *Ph-2/2HbO* the CD1 topological position is
12
13 occupied by His58, not by Tyr55 as previously proposed [13]. CD1 His is also present in *At-*
14
15 *2/2HbO*, whereas in TrHbs this site typically hosts Phe, with the exception of TrHbIIs from *M.*
16
17 *tuberculosis*, *M. avium*, *M. leprae*, *M. smegmatis*, *Streptomyces coelicolor*, *Corynebacterium*
18
19 *diphtheriae* and *T. fusca*, which host Tyr [5,20].
20
21

22
23 A medium polarity distal cavity of about 50 Å³ volume is defined by the porphyrin ring
24
25 and by residues Phe(41)B9, Tyr(42)B10, His(58)CD1, Ile(65)E7, Phe(69)E11 and Trp(109)G8
26
27 (Fig. 3); the cavity hosts two water molecules that form a H-bonded network with the heme
28
29 distal residues (see below). Analysis of the whole *Ph-2/2HbO* crystal structure does not
30
31 highlight a proper protein matrix tunnel(s) connecting the heme distal cavity to the solvent,
32
33 such as those observed in *Mt-TrHbI* [20,21]. This finding is in keeping with the absence of a
34
35 protein-matrix tunnel previously reported for TrHbIIs. TrHbIIs also tend to host a small residue
36
37 at E7 (typically Ala, Ser, or Thr), thus suggesting the an E7 route entry path to facilitate the
38
39 accessibility of diatomic ligands to the heme distal site [2,3,19]. In E7, the residue in *Ph-*
40
41 *2/2HbO* is Ile(65), whose side chain separates the heme distal cavity from the solvent region
42
43 (Fig. 3A). An alternative access to the heme distal cavity might be located between the B, C
44
45 and E helices, however the bulky side chains of Tyr(42)B10, Tyr(55)C5, His(58)CD1 and
46
47 Leu(62)E2 appear to hinder such an entry site in the *Ph-2/2HbO* crystal structure (Fig. 3A).
48
49
50
51
52
53

54 55 56 *Heme pocket* 57

58
59 Both *Ph-2/2HbO* A and B chains display the heme porphyrin ring rotated by 180° around
60
the methinic α - γ meso axis, relative to the common orientation found in (non)vertebrate

1
2 globins. In *Ph-2/2HbO*, the bound heme is stabilized through direct Fe-coordination to
3 proximal His(96)F8, electrostatic interactions with the heme propionates, and van der Waals
4 contacts ($< 4.0 \text{ \AA}$) with 23 residues. In particular, in both chains, propionate-D is stabilized by a
5
6
7 H-bonded salt bridge with Arg(95)F7, and propionate-A is electrostatically coupled to Arg64
8 slightly differently in the two chains (Fig. 3B); moreover, a water molecule provides a H-bond
9 bridge between propionates A and D in the B chain. It is worth noting that in *Ph-2/2HbO* site
10
11
12 83 (within helix Φ), which generally hosts a highly conserved Tyr in TrHbIIs, is occupied by
13
14
15 Phe (Fig. 2), thus impairing the formation of an additional H bond with propionate D.
16
17
18
19
20

21 In the proximal site, Leu92, Phe99, Ile101 and Met141 are mainly involved in van der
22
23
24
25
26
27
28
29
30
31
32
33
34
35
36
37
38
39
40
41
42
43
44
45
46
47
48
49
50
51
52
53
54
55
56
57
58
59
60

Waals contacts with the porphyrin ring. Proximal His(96)F8 is coordinated to the heme iron atom (coordination-bond length of 2.2 \AA in chain A and 2.1 \AA in chain B), with the F8 imidazole ring lying in a staggered azimuthal orientation relative to the heme pyrrole N atoms. Accordingly, the ferrous form showed a $\nu(\text{Fe-His})$ stretching mode at 222 cm^{-1} [14], higher than that of human HbA (214 cm^{-1}), but similar to that of other TrHbs characterized by a staggered orientation of the proximal His imidazole ring [22]. In fact, the staggered orientation, in contrast to the eclipsed orientation observed in HbA [22], is expected to increase the iron-His bond strength.

In the heme distal pocket, Phe(41)B9, Tyr(42)B10, His(58)CD1, Ile(65)E7, Phe(69)E11 and Trp(109)G8 surround the heme-ligated water molecule (Fig. 3B). The His(58)CD1 imidazole ring is parallel to the heme, its orientation being set by a H-bond (2.9 \AA) between the ND1 atom and the carbonyl O_2 atom of Leu(54)C4. At the rear end of the distal pocket, Trp(109)G8, conserved in TrHbIIs and TrHbIIIs, fills the inner part of the heme distal site, preventing further diffusion of ligands away from the heme-Fe coordination site. The Trp(109)G8 indole ring is parallel and in contact with the porphyrin ring at the B and C pyrroles (Fig. 3B).

1
2 The heme distal site is characterized by a highly intertwined H-bonded network, involving
3
4 Tyr(42)B10, His(58)CD1, Trp(109)G8, and two water molecules (W13 and W32 in the A
5
6 chain, W16 and W23 in the B chain; Fig. 3B). In particular, the heme-coordinated water
7
8 molecules (W32 in A and W16 in B chains, with Fe-O 2.2 Å coordination bonds), are H
9
10 bonded to a second distal-site water molecule (W13 in the A chain and W23 in the B chain; 2.6
11
12 Å and 2.5 Å distances, respectively), and to the indole NE1 atom of Trp(109)G8 (3.0-Å and 3.1
13
14 Å distances, respectively). The W13 and W23 water molecules are fully buried in the distal
15
16 site, and are in turn H bonded to the Tyr(42)B10 hydroxyl group (2.8 Å and 2.7 Å,
17
18 respectively) and to the NE2 atom of His(58)CD1 (2.5 Å and 2.6 Å, respectively).
19
20
21
22
23
24

25 *Spectroscopic measurements in solution*

26
27
28 The electronic absorption spectrum of ferric *Ph-2/2HbO* and its second derivative
29
30 spectrum at pH 7.6 (Fig. 4A), characterized by a Soret band at 408 nm, Q bands at 503, 541 and
31
32 570 nm, and a CT1 band at 635 nm, suggests a mixture of high-spin (HS) and low-spin (LS)
33
34 forms. This is confirmed by the corresponding high-frequency RR spectrum (Fig. 4D), which
35
36 clearly indicates a mixture of two forms; a predominant aquo hexa-coordinated HS state (6cHS;
37
38 ν_3 1480, ν_2 1558, ν_{10} 1608 cm^{-1}) and a less populated hexa-coordinated LS state (6cLS; ν_3 1503
39
40 cm^{-1}). These spectra are different from those previously reported for ferric *Ph-2/2HbO* at pH
41
42 7.6 [13] where, likely due to different preparation procedures, multiple LS forms were observed
43
44 (see Materials and Methods). However, as reported in that case, the absorption maxima of the
45
46 LS form are quite unusual, and reminiscent of those of ferric *Chlamydomonas* chloroplast Hb
47
48 [23] and of the hemophore HasA proteins from *Serratia marcescens* and *Pseudomonas*
49
50 *aeruginosa* [24,25]. Nevertheless, they are very different from either a LS His-Fe-His (that
51
52 exhibits well-defined absorption bands at about 535 and 565 nm), or a His-Fe-OH heme
53
54 complex as observed at alkaline pH (see below) [26].
55
56
57
58
59
60

1
2 As suggested by the crystal structure, two distal-site residues may be involved in
3
4 generating the 6cLS state, i.e. His(58)CD1 and Tyr(42)B10 (Fig. 3B). In order to check
5
6 whether a Tyr might be coordinated to the heme-Fe atom, RR excitation in the visible region
7
8 was performed since the characteristic vibrational frequencies of bound phenolate can often be
9
10 identified by excitation in the tyrosinate–Fe(III) charge transfer band (near 500 nm) [27]. As
11
12 shown in Fig. 5, upon excitation in the visible region at pH 7.6, three bands at 590, 1312 and
13
14 1509 cm^{-1} (which are polarized, data not shown) are enhanced, becoming particularly evident
15
16 upon excitation at 514.5 nm. These bands are assigned to the $\nu(\text{Fe}-\text{O}_{\text{Tyr}})$, $\nu_{\text{Tyr}}(\text{C}-\text{O})$, and
17
18 $\nu_{\text{Tyr}}(\text{C}=\text{C})$ tyrosinate modes, respectively, which are not present in the spectrum upon excitation
19
20 at 413.1 nm. The band around 590 cm^{-1} , due to the stretching mode of the covalent bond
21
22 between the heme-Fe atom and the Tyr phenolic O, $\nu(\text{Fe}-\text{O}_{\text{Tyr}})$, is of special interest, since its
23
24 frequency is highly sensitive to the Tyr protonation state. Table 2 reports the frequencies of the
25
26 phenolate modes observed in a number of heme-Fe tyrosinate complexes in different proteins,
27
28 for comparison with those presented here; such frequencies differ slightly from those reported
29
30 in a previous study on *Ph-2/2HbO* [13]. Based on previously reported UV and visible RR
31
32 spectra (Table 2, [29]), the frequency at 590 cm^{-1} observed in *Ph-2/2HbO* is consistent with a
33
34 deprotonated Tyr.
35
36
37
38
39
40
41

42 In agreement with the electronic absorption and RR spectra, the *Ph-2/2HbO* X-band EPR
43
44 spectrum at pH 7.6 displays an axial HS signal ($g_{\perp} \sim 6.0$, $g_{\parallel} \sim 2.0$) and only one rhombic LS form
45
46 ($g = 2.95, 2.26, 1.49$) (Fig. 4B). The LS g values differ from those normally observed for His–
47
48 Fe–Tyr axial coordination, where the tyrosinate is not H-bonded, but also from the values
49
50 reported for His-Fe-His and His-Fe-OH LS signals (Table S1). However, they are similar to
51
52 those of the human serum albumin–ibuprofen complex (2.93, 2.27, 1.55) [32] and the HasA
53
54 proteins from *S. marcescens* and *P. aeruginosa* ($g = 2.86, 2.21, 1.71$) [24,25]. In both cases, a
55
56 nearby His serves as H-bond acceptor to stabilize the phenolate ligand. Hence, by analogy with
57
58 HasA, and in agreement with the electronic absorption and RR spectra, the *Ph-2/2HbO* LS
59
60

1
2 form is proposed to host His–Fe–Tyr axial coordination, with a deprotonated Tyr strongly H-
3
4 bonded to a nearby residue that stabilizes the phenolate. Based on sequence alignments (Fig. 2)
5
6 and the location of heme distal residues resulting from the crystal structure (Fig. 3B),
7
8 Tyr(42)B10 is proposed as the sixth heme-Fe ligand in the *Ph-2/2HbO* LS form. Notably,
9
10 analysis of the aquo-met *Ph-2/2HbO* crystal structure (which displays a heme-coordinated
11
12 water molecule) does not allow identification of a distal residue acting as the sixth heme-Fe
13
14 ligand, as observed in the protein 6cLS form in solution. In this respect, attempts to produce a
15
16 *Ph-2/2HbO* variant mutated at the B10 site (replacing Tyr42 with Phe) yielded a purified
17
18 greenish globin, likely due to the presence of heme-d [33], which compromised the
19
20 spectroscopic analyses. Attempts to generate the apoprotein followed by reconstitution *in vitro*
21
22 with hemin proved unsuccessful in this mutant, but also in a mutant bearing the
23
24 Trp(109)G8→Phe mutation.
25
26
27
28
29

30 The RR bands assigned to tyrosinate modes disappear at alkaline pH (Fig. 5), as at this pH
31
32 (>10) the protein is characterized by a hydroxyl ion bound to the heme-Fe atom. The
33
34 absorption spectrum is characteristic of a mixture of 6cHS and 6cLS forms (Soret band at 414
35
36 nm, Q bands at 545 and 587 nm, and a weak CT1 band at 610 nm, Fig. 4A), consistent with the
37
38 observed high-frequency RR spectrum that displays a predominant 6cLS form (ν_3 1501, ν_2
39
40 1579, ν_{37} 1604, ν_{10} 1638 cm^{-1}) and a weak 6cHS form (ν_3 1477 cm^{-1}). It is worth noting that the
41
42 high-frequency RR spectrum also reveals the presence of a 5cHS form at alkaline pH (ν_3 1491
43
44 cm^{-1}) (Fig. 4D) (see below). At alkaline pH the relative intensities of the γ_6 (at 336 cm^{-1}),
45
46 propionyl (368 and 380 cm^{-1}) and vinyl bending (410 and 422 cm^{-1}) modes are significantly
47
48 reduced as compared to pH 7.6 (Fig. 4C), suggesting that at pH > 10 the H-bonding interactions
49
50 with the propionyl groups (observed in the X-ray structure) are weakened [34]. Figs. S2-S5 and
51
52 Tables S2-S5 in the supplemental materials report the curve fitting analysis of the RR spectra
53
54 shown in Fig. 5 and the complete vibrational assignment.
55
56
57
58
59
60

1
2 In agreement with the RR data, in the EPR spectrum at alkaline pH the LS signal
3
4 corresponding to His–Fe–Tyr axial coordination is almost absent ($g = 2.95, 2.26, 1.49$), being
5
6 replaced by a new LS signal ($g = 2.65, 2.19, 1.82$) (Fig. 4B), typical of hydroxyl heme LS
7
8 forms (Table S1, [35]).
9

10
11 Fig. 6 compares the low-frequency RR spectra of *Ph-2/2HbO* at alkaline pH in H_2O , D_2O
12 and $H_2^{18}O$ buffered solutions, at 12 K (Fig. 6A-B) and 298 K (Fig. 6C-D). The 6cHS and 6cLS
13
14 forms exist in a thermal spin-state equilibrium at room temperature, being converted to almost
15
16 pure 6cLS heme at 12 K with a small population of 5cHS still present (Fig. S6). At 12 K the
17
18 resolution of the bands is higher, enabling the weak $\nu(\text{Fe-OH})$ bands to be more easily
19
20 identified through their sensitivity to ^2H and ^{18}O isotopic substitution. The two isotope-
21
22 sensitive bands observed at 528 and 568 cm^{-1} (at 12 K), (525 and 570 cm^{-1} at 298 K) are
23
24 assigned to two $\nu(\text{Fe-OH})$ stretching modes. The band at 528 cm^{-1} is assigned to a His-Fe-OH⁻
25
26 6cLS form. Its frequency, about 20- cm^{-1} lower than that observed in met-Mb and met-Hb [36],
27
28 is indicative of strong H bonds between the OH⁻ ligand and distal residues. In fact, with an
29
30 increase of the H-bond strength, a decrease of the force constant of the Fe-OH bond, with
31
32 concomitant decrease of the $\nu(\text{Fe-OH})$ stretching frequency, is expected. Upon isotopic
33
34 substitution in D_2O buffer, this band up-shifts by 6 cm^{-1} rather than displaying the expected
35
36 down-shift due to the increased mass of the Fe-OD oscillator relative to Fe-OH. A similar
37
38 behaviour has been previously observed in horseradish peroxidase (HRPC) [36] (Table 3),
39
40 where distal Arg38 appears essential for stabilization of the OH⁻ ligand and distal His(42)E7
41
42 acts as a H-bond acceptor [43]. Moreover, similar to HRPC [36], upon isotopic substitution in
43
44 D_2O at room temperature (Fig. S7), a decrease in intensity and a small frequency change are
45
46 observed for the bending mode of the propionyl group at 367 cm^{-1} , indicating an alteration in
47
48 the H-bonded network induced by the different strengths of H- and deuterium-bonds interacting
49
50 with the heme ligand. The corresponding band of the 6cHS (observed only at room
51
52 temperature) has not been identified.
53
54
55
56
57
58
59
60

1
2 The band at 568 cm^{-1} down-shifts to 554 and 549 cm^{-1} in D_2O and H_2^{18}O , respectively. It is
3
4 noteworthy that the frequency of this band is much higher than those typical of 6cLS and 6cHS
5
6 Fe-OH forms. In analogy with the His93Gly Mb mutant ($\nu(\text{Fe-OH})$ at 575 cm^{-1}) and *Scapharca*
7
8 *inaequivalvis* Hb [41,42], it is assigned to a 5cHS Fe-OH form, uncommon in heme proteins.
9
10 Such an assignment implies that the proximal His-Fe bond must be ruptured at alkaline pH. The
11
12 alkaline transition is fully reversible, hence this form does not result from denaturation of the
13
14 protein. Table 3 lists the $\nu(\text{Fe-OH})$ frequencies observed in a number of reference heme
15
16 proteins at alkaline pH. The 6cLS form, whose frequency is similar to that observed in *Mt-*
17
18 *2/2HbO* [37], is characterized by strong H bonds between OH^- and distal residues. However,
19
20 similar to TrHb-I of the cyanobacterium *Synechocystis* [40], at alkaline pH *Ph-2/2HbO* shows
21
22 the presence also of a 5cHS characterized by the rupture of the Fe-His proximal ligand.
23
24
25
26
27

28 Fig. 7 compares the RR spectra as a function of pH between neutral and alkaline pH,
29
30 including the intermediate pH 8.5 value, which corresponds to the pH used in the crystal-
31
32 structure analysis. While the electronic absorption spectrum at pH 8.5 is almost identical (data
33
34 not shown) to that at pH 7.6 (Fig. 4A), at increasing pH a general reduction in the low-
35
36 frequency RR spectrum intensity (normalized on the ν_7 mode (678 cm^{-1})) takes place (Fig. 7A).
37
38 The most evident changes are the marked decrease in relative intensity of the bending modes in
39
40 the $330\text{-}430\text{ cm}^{-1}$ region and, in the high frequency region, the up-shift of the ν_4 mode by 1 cm^{-1}
41
42 from pH 7.6 to 8.5 (Fig. 7B). Therefore, we can conclude that at pH 8.5 the spectrum is
43
44 intermediate between those at pH 7.6 and at pH 10.9, thus displaying a small Fe-OH LS
45
46 population. This result is in agreement with the results from the X-ray structure, where a heme-
47
48 Fe coordinated water molecule (W13 in chain A, and W23 in chain B) is involved in a distal H-
49
50 bonded network, suggesting that this molecule may assume a degree of OH^- 6cLS character.
51
52
53
54
55
56
57
58
59
60

Molecular Dynamic Simulations

1
2 MD simulations of ferrous *Ph-2/2HbO*, in the absence of any heme distal ligand, show that
3
4 water molecules can access the heme distal cavity and be stabilized through a H-bond network
5
6 based on the distal residues Tyr(42)B10, His(58)CD1 and Trp(109)G8 (Fig. S8), in agreement
7
8 with the X-ray crystal structure (Fig. 3B). Besides mapping the water dynamics in the heme
9
10 distal site, during MD simulation it was possible to analyze the dynamic behaviour of the
11
12 residues surrounding the heme. In particular, we focused our attention on Tyr(42)B10 that, on
13
14 the basis of the RR experiments, is suggested to be coordinated to the heme-Fe atom. In our
15
16 MD simulation, Tyr(42)B10 is too far from the iron to be considered a candidate to occupy the
17
18 sixth coordination site. This is similar to other well studied members of the TrHbII family, such
19
20 as *Bs-2/2HbO*, *Tf-2/2HbO* and *Mt-2/2HbO* [44-46], where no endogenous hexa-coordination
21
22 was observed (Fig. S9). As the currently accessible timescales of MD simulations inherently
23
24 limit the extent of conformational space that can be sampled, an alternative conformation, with
25
26 Tyr(42)B10 coordinated to the heme-Fe atom cannot be ruled out at longer simulation times. A
27
28 large structural rearrangement would however be required to attain a conformation compatible
29
30 with endogenous heme hexa-coordination based on Tyr(42)B10.
31
32
33
34
35
36

37 MD simulations of the *Ph-2/2HbO* CO (Fig. 8A) and O₂ (Fig. 8B) complexes show that
38
39 both ligands are stabilized by a strong H bond to Trp(109)G8, and a weaker one to Tyr(42)B10
40
41 (Figs. 8C-D) with the interaction between O₂ and Trp(109)G8 (Fig. 8D) more stable than that
42
43 between CO and Trp(109)G8 (Fig. 8C). The important role of Trp(109)G8 in ligand
44
45 stabilization has been previously observed in other TrHbIIs, e.g. *Bs-2/2HbO* [45,47], *Tf-*
46
47 *2/2HbO* [46], and *Mt-2/2HbO* [37,44]. No significant interactions of the CO ligand with
48
49 His(58)CD1 are apparent from the simulations (data not shown).
50
51
52
53

54 A detailed analysis of possible ligand migration pathways and associated tunnel/cavities
55
56 within the protein matrix was performed using the Implicit Ligand Sampling (ILS) method. A
57
58 comparison between cavities identified by the X-ray and the MD structures is provided in Fig.
59
60 9. Even though no widely open tunnels were identified, a possible pathway for ligand migration

1
2 at the E7 gate was shown by MD simulations (Fig. 9). In particular, two on-pathway docking
3
4 sites were found for the CO ligand: the first cavity is located over the heme-Fe atom (CO)₁, as
5
6 suggested by the crystal structure, while the second, (CO)₂, originates from rearrangements of a
7
8 few residues with respect to the X-ray structure, sampled along the MD simulation. This
9
10 structural rearrangement involves residues Ile(65)E7, Val(68)E10 and Phe(69)E11 that,
11
12 together with Tyr(42)B10, define a possible ligand-entry pathway located between helices E
13
14 and F.
15
16
17
18
19
20

21 Discussion

22
23 Since only about half of the 2200 bacterial genomes sequenced so far include genes
24
25 encoding globins, it appears that these proteins may not always be required to sustain bacterial
26
27 physiology; on the other hand, many bacterial genomes comprise more than one globin gene
28
29 [1]. The occurrence of the TrHbII + FHb combination in 1162 genomes poses the question
30
31 whether the function of TrHbIIs is necessarily linked to the NO-dioxygenase activity of FHbs.
32
33 Different double and ternary combinations of TrHbI, TrHbII, and TrHbIII with FHb are
34
35 uncommon. *PhTAC125* is the only example described so far in which genes encoding a FHb
36
37 and three TrHbs coexist [11], a feature potentially related to cold environments. In fact, gene
38
39 redundancy has been shown to entail mechanisms that warrant expression of an essential
40
41 function [48]; such redundancy may be perceived as a systemic adaptation to extreme
42
43 environments.
44
45
46
47
48

49 The ability of an organism to survive and grow in the cold depends on a number of
50
51 adaptive strategies, finalized to maintaining vital cellular functions at low temperatures [49]. In
52
53 addition to adaptations at the cellular level, to preserve their functions proteins must maintain a
54
55 balance between conformational stability and flexibility under the selected environmental
56
57 conditions. The apparent flexibility of proteins from cold-adapted organisms would compensate
58
59 for the low kinetic energy of solvent and molecules in their environment. A reduction of
60

1
2 surface, of inter-domain or inter-subunit ionic interactions, a decreased number of H bonds and
3
4 salt bridges are all key mechanisms that can lead to increased conformational flexibility [50].
5
6 Several studies indicate that minor structural modifications are sufficient to modify the intrinsic
7
8 stability of cold-adapted proteins, and that local rather than global flexibility may play an
9
10 important role in cold adaptation [51].
11
12

13
14 A hint of enhanced plasticity in cold-adapted *Ph-2/2HbO* was provided by comparative
15
16 analysis with other members of the family, e.g. *Tf-2/2HbO* and *Mt-2/2HbO*. RMSF analysis
17
18 over 100 ns of MD simulations at 300 K on all three proteins highlighted significant
19
20 conformational fluctuations in the *Ph-2/2HbO* EF loop (residues 79-83) compared to the other
21
22 two TrHbIIs (Fig. S10). Moreover, comparative analysis of structural adaptation in many cold-
23
24 adapted globins, such as Antarctic fish Hbs and neuroglobins, shows higher flexibility in the
25
26 CD and EF regions [52-55]. Such findings suggest that helix F and its surroundings may be
27
28 involved in conferring localized flexibility in cold-adapted globins. The RR data at alkaline pH
29
30 also strongly support the evidence of an unusually flexible proximal heme pocket in *Ph-2/2HbO*.
31
32 In fact, the observation of the uncommon 5cHS Fe-OH form at alkaline pH implies
33
34 that the proximal HisF8-Fe bond must be severed at this pH without denaturing the protein,
35
36 since the alkaline transition is completely reversible and the protein fully regains its native state
37
38 upon return to neutral pH.
39
40
41
42
43

44
45 The comparison of the spectroscopic and crystallographic properties of *Ph-2/2HbO*, here
46
47 reported, provides additional information regarding protein flexibility. In fact, the spectroscopic
48
49 observation of a mixture of an aquo-met 6cHS species and a 6cLS component, the latter due to
50
51 ligation of Tyr(42)B10 to the heme-Fe atom but not detected by the crystal structure, indicates
52
53 that heme coordination is affected by the physical and/or environmental conditions experienced
54
55 by the protein. Such coexistence of two different heme coordination states is in keeping with
56
57 the proposed conformational flexibility of the heme pocket of this cold-adapted TrHbII.
58
59 Differences in heme coordination between solution and crystalline states have been previously
60

1
2 described in various hemoproteins [56,57]. In addition, analogous results have been reported in
3
4 *B. subtilis* dye-decolourising peroxidase. The 6cLS state of this protein is the most populated in
5
6 solution, whereas a 6cHS state is mainly detected in the crystal, such differences being related
7
8 to a highly flexible heme pocket [58]. In such a general context, it can be proposed that, in the
9
10 *Ph-2/2HbO* case, the crystallization conditions promote attainment of the aquo-met 6cHS
11
12 species, or select it for crystal growth as the most populated/stable of the two forms.
13
14

15
16 In terms of ligand accessibility to the active site, the E7 pathway located between helices E
17
18 and F was already observed in related TrHbIIs, e.g. *Tf-2/2HbO* and *Mt-2/2HbO*, suggesting
19
20 similar k_{on} values (10^4 - 10^5 M⁻¹ s⁻¹) for the predominant CO-rebinding process in these proteins
21
22 [14,15,59,60]. Nevertheless, the crystallographic and MD analyses presented in this work do
23
24 not provide an explanation for the biphasic nature of CO-rebinding kinetics of *Ph-2/2HbO*
25
26 [14,15]. Moreover, the RR of the *Ph-2/2HbO*-CO complex indicates the presence of a CO
27
28 conformer in which polar interactions with the surrounding residues of the distal cavity are
29
30 absent or very weak [14].
31
32
33

34
35 Taken together, these data depict a flexible architecture in the heme pocket of *Ph-2/2HbO*,
36
37 hardly reported for other globins. The results highlight the unique adaptive structural properties
38
39 of the protein that enhance its overall flexibility, as recently demonstrated by its resistance to
40
41 pressure-induced stress [15]. Although some of these adaptive mechanisms are undoubtedly
42
43 species-specific, the remarkable access of *Ph-2/2HbO* to unusual conformations may represent
44
45 a molecular property encoded in the TrHbII structure to face the dynamic and functional
46
47 requirements posed by the Antarctic environment.
48
49
50

51 52 53 **Materials and Methods**

54 *Protein expression and purification*

55
56 The *PSHAa0030* gene encoding *Ph-2/2HbO* was cloned as previously described [10]. The
57
58 previously used fermentor [13] was replaced by small-scale (200 ml) cultures in shake flasks to
59
60

1
2 improve the quality of expression. In fact, production of the protein under strong oxygenation
3
4 conditions may have given rise to the multiple LS forms observed previously [13]. For
5
6 overexpression of *Ph-2/2HbO* in *E. coli* BL21(DE3), a single colony carrying the plasmid
7
8 construct (pET28a-*Ph-2/2HbO*) was inoculated in LB medium supplemented with kanamycin
9
10 (50 µg/ml), in the presence of 0.3 mM D-aminolevulinic acid, and allowed to grow at 25 °C
11
12 until A₆₀₀ reached 0.6 OD. The culture was then induced with 1 mM isopropyl-β-D-
13
14 thiogalactopyranoside, further incubated for 16 h at 25 °C and shaken at 150 rpm. The
15
16 expression of the cloned protein was monitored after running the cell lysate of recombinant
17
18 strains in 15% SDS-PAGE followed by Coomassie Brilliant Blue staining.
19
20
21
22

23 To purify *Ph-2/2HbO*, the frozen cells, previously harvested by centrifugation at 4 °C,
24
25 were thawed, suspended in 50 mM Tris-HCl pH 7.6, 1.0 mM EDTA, 1.0 mM phenyl-methyl-
26
27 sulfonyl-fluoride and protease-inhibitor cocktail (SIGMA P8465), and disrupted in a French
28
29 press until the supernatant was reddish and clear. The cell debris was removed by
30
31 centrifugation at 30,000 rpm for 1 h at 4 °C. The supernatant was loaded onto an anion-
32
33 exchange column (Q Sepharose Fast Flow, GE Healthcare Biosciences), equilibrated with 20
34
35 mM Tris-HCl pH 7.6 and 1.0 mM EDTA (Akta Explorer system, GE Healthcare Biosciences,
36
37 Amersham Biosciences Ltd, UK). *Ph-2/2HbO* was eluted with a NaCl gradient (from 0 to 0.25
38
39 M) in 20 mM Tris-HCl pH 7.6, 1.0 mM EDTA. The eluted fractions were collected on the
40
41 basis of the heme and protein absorbance at 407 and 280 nm, respectively. The pooled fractions
42
43 were concentrated and loaded onto a second anion-exchange column (HiTrap Q Sepharose XL,
44
45 GE Healthcare Biosciences) equilibrated with 20 mM Tris-HCl pH 7.6 and 1.0 mM EDTA.
46
47 *Ph-2/2HbO* was eluted with a NaCl gradient (from 0 to 0.25 M) in 20 mM Tris-HCl pH 7.6,
48
49 1.0 mM EDTA. The collected protein was concentrated, dialysed against 50 mM MES pH 6.0,
50
51 and further purified with a SP (sulfopropyl) Sepharose Fast Flow cation-exchange column (GE
52
53 Healthcare Biosciences) equilibrated with 50 mM MES pH 6.0. The protein was eluted with a
54
55 NaCl gradient from 0 to 0.50 M. A fourth purification step (strong anion-exchanger, MonoQ,
56
57
58
59
60

1
2 GE Healthcare Biosciences) was necessary to obtain the protein at 98% purity, as judged from
3
4 SDS-PAGE.
5

6
7 *Ph-2/2HbO* was isolated as a cleaved form, as confirmed by mass spectrometry (data not
8
9 shown), devoid of the first 19 N-terminal residues. This cleaved form is likely the result of
10
11 proteolysis of the full-length protein by trace amounts of proteases co-purified with the cold-
12
13 adapted globin [10]. It should be recalled that previous *in vivo* experiments demonstrated that
14
15 deletion of the N-terminal segment does not impair the NO scavenging activity of *Ph-2/2HbO*
16
17 [16]. Throughout the following, the truncated form of the protein (i.e. devoid of the first 19 N-
18
19 terminal residues) will simply be referred to as *Ph-2/2HbO*.
20
21
22
23
24

25 26 *Crystallization and data collection*

27
28 Crystals of aquo-met *Ph-2/2HbO* (protein concentration 30 mg/ml) were grown at 4 °C by
29
30 the vapour-diffusion technique, using 8% PEG 8000 and 0.1 M Tris–HCl pH 8.5 as precipitant
31
32 solution. Crystals grew after several months as bunches of rods from which single elongated
33
34 prismatic crystals (of about $0.15 \times 0.15 \times 0.4 \text{ mm}^3$) could be isolated; these were cryoprotected
35
36 with 15% PEG 8000, 0.1 M Tris–HCl pH 8.5, and 20% glycerol prior to data collection at 100
37
38 K. The crystals diffracted up to 2.21 Å resolution on beamline ID23-1, at the ESRF synchrotron
39
40 (Grenoble, France), and were shown to belong to the orthorhombic space group $P2_12_12_1$, with
41
42 unit cell parameters $a = 42.9 \text{ Å}$, $b = 72.3 \text{ Å}$, $c = 88.3 \text{ Å}$, $\alpha = \beta = \gamma = 90^\circ$ (Table 1). Calculation
43
44 of the packing parameter ($V_M = 2.41 \text{ Å}^3/\text{Da}$, 49% solvent content) indicated the presence of
45
46 two *Ph-2/2HbO* molecules in the crystal asymmetric unit. Raw diffraction data were processed
47
48 using Mosflm [61] and SCALA [62].
49
50
51
52
53

54 55 56 57 *Structure determination and refinement*

58
59 Solution of the 3D structure was achieved through molecular-replacement techniques,
60
using the web-server Caspr (<http://www.igs.cnrs-mrs.fr/Caspr2/>; [63]). The crystal structure of

1
2 *At*-2/2HbO (PDB code: 2XYK) was used as the search model. Several cycles of manual
3
4 rebuilding using the program COOT [64], and refinement (rigid body and restrained
5
6 refinement) using the program REFMAC5 [65], were carried out to improve the initial electron
7
8 density for the two independent *Ph*-2/2HbO molecules (A and B chains). At the end of
9
10 refinement, no electron density was present for residues 20-21 of *Ph*-2/2HbO in both A and B
11
12 chains, and 62 water molecules were located through difference Fourier maps (Table 1). The
13
14 programs Procheck [17] and Surfnet [66] were used to assess the model stereochemical quality
15
16 and to search for protein matrix cavities. Atomic coordinates and structure factors have been
17
18 deposited in the Protein Data Bank (**PDB ID: 4UUR** and **R4UURSF**, respectively).
19
20
21
22
23
24

25 *Spectroscopic measurements*

26
27
28 The *Ph*-2/2HbO samples at pH 7.6 and 8.5 were prepared in 0.1 M Tris–HCl, and those at
29
30 pH 10.9 in 0.1 M CAPS. Protein concentrations in the range 10-70 μM were used for electronic
31
32 absorption and RR samples. Sample concentration for low-temperature RR was between 30 and
33
34 100 μM . The concentration of the EPR samples was 90 μM . The protein concentration was
35
36 estimated on the basis of the molar absorptivity, $\varepsilon = 131 \text{ mM}^{-1} \text{ cm}^{-1}$ at 408 nm.
37
38
39

40
41 The hydroxyl complex in isotopically enriched water was prepared by adding 5 μL of *Ph*-
42
43 2/2HbO in 0.02 M natural abundance buffer, to 50 μL of 0.1 M CAPS buffer prepared with
44
45 D_2O or H_2^{18}O to obtain a final pD 11.0 and pH 10.9, respectively. Isotopically enriched water
46
47 (H_2^{18}O) (95%) and D_2O (99.8%) was purchased from Cambridge Isotope Laboratories (USA)
48
49 and Merck AG (Darmstadt, Germany), respectively. All chemicals were of analytical or reagent
50
51 grade and were used without further purification.
52
53

54
55 Electronic absorption spectra were recorded with a double-beam spectrophotometer
56
57 (Varian Cary 5) using a 1-mm quartz cuvette and a 5-mm NMR tube at a scan rate of 600 nm
58
59 min^{-1} . The RR spectra were obtained using a 5-mm NMR tube and by excitation with the 413.1
60
nm line of a Kr^+ laser (Innova 300 C, Coherent, Santa Clara, CA, USA), and the 496.5 nm and

1
2 514.5 nm lines of an Ar⁺ laser (Innova 90/5, Coherent). The backscattered light from a slowly
3
4 rotating NMR tube was collected and focused into a triple spectrometer (consisting of two
5
6 Acton Research SpectraPro 2300i working in the subtractive mode, and a SpectraPro 2500i in
7
8 the final stage), equipped with a liquid nitrogen-cooled CCD detector (Roper Scientific
9
10 Princeton Instruments). Absorption spectra were measured both prior to and after RR
11
12 measurements to ensure that no degradation had taken place. The low-temperature experiments
13
14 were carried out using an Air Products Displex closed-cycle He refrigerator with automatic
15
16 temperature control. For the low-temperature RR measurements, 20 μ L of the protein solution
17
18 was placed on the copper cold finger of the refrigerator at 90 K, under nitrogen flow, and the
19
20 RR spectra were recorded at 12 K. The RR spectra were calibrated with indene, n-pentane,
21
22 dimethylsulfoxide, acetonitrile, and carbon tetrachloride as standards to an accuracy of 1 cm^{-1}
23
24 for intense isolated bands.
25
26
27
28
29

30 All RR measurements were performed several times under the same conditions to ensure
31
32 reproducibility. To improve the signal-to-noise ratio, a number of spectra were accumulated
33
34 and summed only if no spectral differences were noted. All spectra were baseline corrected.
35
36

37 To determine peak bandwidth and positions, a curve-fitting program (Lab Calc; Galactic)
38
39 was used to simulate the spectra using a Lorentzian line shape. The frequencies of the bands
40
41 were optimized with an accuracy of 1 cm^{-1} and the bandwidths with an accuracy of 0.5 cm^{-1} .
42
43

44 EPR spectra were recorded with a Bruker Elexys E500, equipped with an NMR
45
46 gaussmeter and a microwave frequency counter. An Oxford Instruments ESR 900 cryostat was
47
48 used to obtain low temperatures. Spectra were recorded under non-saturating conditions at 5 K,
49
50 1 mW microwave power, and 1 mT modulation amplitude. The g-values were determined by
51
52 careful visual inspection of the spectra.
53
54
55
56
57

58 *Molecular Dynamic Simulations*

59
60

1
2 Simulations were performed starting from the crystal structure of *Ph-2/2HbO* reported
3 herein. Three protein-ligand complexes, displaying CO, hydroxide anion, or molecular O₂
4 ligands bound to the heme-Fe atom, were built and simulated. The ligands were added at the
5 distal site, bound to Fe(III) (hydroxide) and to Fe(II) (carbon monoxide and O₂), according to
6 the equilibrium structure in an isolated model system. Quantum Mechanics (QM) calculations
7 were performed at the Density Functional Theory (DFT) level (with the Perdew-Burke-
8 Ernzerhof functional, PBE, and 6-31G** basis sets), taking into account structural features of
9 the distal-site environment. The charges and parameters of the Fe(III) heme-hydroxide and the
10 Fe(II) heme-CO and heme-O₂ adducts were determined by the standard procedure, i.e. partial
11 charges were computed using the restricted electrostatic potential (RESP) recipe and DFT
12 electronic-structure calculations with the PBE functional and 6-31G** basis sets. The
13 calculations were performed in the high-spin (HS) state for the hydroxide adduct, and in the
14 low-spin (LS) state for the oxygenated species. Equilibrium distances and angles, as well as
15 force constants, were computed using the same methods and basis set used for the computed
16 charges. The parm99 force field implemented in AMBER12 was used to describe the protein
17 [67]. The protein complexes were then immersed in a pre-equilibrated octahedral box of ~4910
18 TIP3P water molecules using the tLEaP module of the AMBER12 package [67]. Periodic
19 boundary conditions with a 9 Å cutoff and Ewald sums were used for treating long-range
20 electrostatic interactions. The SHAKE algorithm [68] was used to keep bonds involving H
21 atoms at their equilibrium length, allowing the use of a 2-fs time step for the integration of
22 Newton's equations. The temperature and pressure were kept constant with a Berendsen
23 thermostat and barostat, respectively, as implemented in the AMBER12 package [67]. The His
24 tautomeric state and protonation (Nε-H, Nδ-H, His⁺) were carefully analyzed for each of the six
25 His (His58, His87, His89, His96, His140 and His145), and set to favour the H-bond network
26 suggested by the experimental crystal structure. The equilibration protocol consisted of (i)
27 slowly heating the whole system from 0 to 300 K for 20 ps at constant volume, with harmonic
28
29
30
31
32
33
34
35
36
37
38
39
40
41
42
43
44
45
46
47
48
49
50
51
52
53
54
55
56
57
58
59
60

1
2 restraints of 80 Kcal/ mol Å² for all C α atoms, (ii) pressure equilibration of the entire system
3
4 simulated for 1 ns at 300 K with the same restrained atoms. After these two steps,
5
6 unconstrained 200 ns of MD simulations at constant temperature (300 K) were performed. All
7
8 structures were stable during the simulations, as determined by RMSD calculation, depicted in
9
10 Figs. S11 and S12.
11
12

13 14 15 16 *Analysis of the small ligand migration free-energy profiles along the protein tunnel*

17
18 The free energy of the CO migration process within the protein matrix was computed by
19
20 the ILS approach that uses pre-computed MD simulations in the absence of the ligand and
21
22 incorporates it afterwards [69]. This method has been thoroughly tested in heme proteins [70].
23
24 ILS calculations were performed in a rectangular grid (0.5 Å resolution) that includes the whole
25
26 simulation box (i.e. protein and solvent), using the CO molecule as a probe. Calculations were
27
28 performed on 5,000 frames taken from the last 180 ns of simulation time. The values for grid
29
30 size, resolution and frame numbers have been thoroughly tested in a previous study [70].
31
32
33
34
35
36
37
38
39

40 **Acknowledgements**

41
42 The authors wish to thank the Centre de Ressources Biologiques de l'Institut Pasteur,
43
44 Paris, France (<http://www.crbip.pasteur.fr>) for supplying the *P. haloplanktis* CIP 108707 strain.
45
46 This study was carried out in the framework of the SCAR programme “Antarctic Thresholds–
47
48 Ecosystem Resilience and Adaptation” (AnT-ERA). It was financially supported by the Italian
49
50 National Programme for Antarctic Research (PNRA), the Italian Ministero dell'Istruzione,
51
52 dell'Università e della Ricerca (MIUR) (PRIN 2007SFZXXZ7, “Structure, function and
53
54 evolution of heme proteins from Arctic and Antarctic marine organisms: cold adaptation
55
56 mechanisms and acquisition of new functions”) (to G.S and C.V.). J.P.B. holds a CONICET
57
58 PhD fellowship. L.B. is a Pew Latin American Fellow. D.A.E. and L.B. are members of
59
60

1
2 CONICET. We thank the ESRF and EMBL-Grenoble staff for assistance and support using the
3
4 beam line ID23-1, and Dr Maria Fittipaldi for provision of EPR facilities and assistance in
5
6 recording the spectra.
7
8
9

10 **Author contributions**

11
12 All authors conceived and designed the experiments. DG, AP, JPB, LB, EC, BDH, AR
13
14 performed the experiments. All authors analyzed the data, and contributed
15
16 reagents/materials/analysis tools. DG, AP, DE, MN, GS, MB, CV wrote the paper.
17
18
19
20
21
22
23
24
25
26
27
28
29
30
31
32
33
34
35
36
37
38
39
40
41
42
43
44
45
46
47
48
49
50
51
52
53
54
55
56
57
58
59
60

References

1. Vinogradov S, Tinajero-Trejo M, Poole RK & Hoogewijs D (2013) Bacterial and archaeal globins - a revised perspective. *Biochim Biophys Acta* **1834**, 1789–1800.
2. Vuletich DA & Lecomte JT (2006) A phylogenetic and structural analysis of truncated hemoglobins. *J Mol Evol* **62**, 196–210.
3. Pesce A, Bolognesi M & Nardini M (2013) The diversity of 2/2 (truncated) globins. *Adv Microb Physiol* **63**, 49–78.
4. Milani M, Savard PY, Ouellet H, Ascenzi P, Guertin M & Bolognesi M (2003) A TyrCD1/TrpG8 hydrogen bond network and a TyrB10TyrCD1 covalent link shape the heme distal site of *Mycobacterium tuberculosis* hemoglobin O. *Proc Natl Acad Sci USA* **100**, 5766–5771.
5. Bonamore A, Ilari A, Giangiacomo L, Bellelli A, Morea V & Boffi A (2005) A novel thermostable hemoglobin from the actinobacterium *Thermobifida fusca*. *FEBS J* **272**, 4189–4201.
6. Giangiacomo A, Ilari L, Boffi A, Morea V & Chiancone E (2005) The truncated oxygen-avid hemoglobin from *Bacillus subtilis*: X-ray structure and ligand binding properties. *J Biol Chem* **280**, 9192–9202.
7. Ilari A, Kjelgaard P, von Wachenfeldt C, Catacchio B, Chiancone E & Boffi A (2007) Crystal structure and ligand binding properties of the truncated hemoglobin from *Geobacillus stearothermophilus*. *Arch Biochem Biophys* **457**, 85–94.
8. Pesce A, Nardini M, Labarre M, Richard C, Wittenberg JB, Wittenberg BA, Guertin M & Bolognesi M (2011) Structural characterization of a group II 2/2 hemoglobin from the plant pathogen *Agrobacterium tumefaciens*. *Biochim Biophys Acta* **1814**, 810–816.
9. Reeder BJ & Hough MA (2014) The structure of a class 3 nonsymbiotic plant haemoglobin from *Arabidopsis thaliana* reveals a novel N-terminal helical extension. *Acta Crystallogr D Biol Crystallogr* **70**, 1411–1418.

- 1
2
3
4
5
6
7
8
9
10
11
12
13
14
15
16
17
18
19
20
21
22
23
24
25
26
27
28
29
30
31
32
33
34
35
36
37
38
39
40
41
42
43
44
45
46
47
48
49
50
51
52
53
54
55
56
57
58
59
60
10. Giordano D, Parrilli E, Dettai A, Russo R, Barbiero G, Marino G, Lecointre G, di Prisco G, Tutino L & Verde C (2007) The truncated hemoglobins in the Antarctic psychrophilic bacterium *Pseudoalteromonas haloplanktis* TAC125. *Gene* **398**, 69–77.
 11. Giordano D, Coppola D, Russo R, Tinajero-Trejo M, di Prisco G, Lauro F, Ascenzi P & Verde C (2013) The globins of cold-adapted *Pseudoalteromonas haloplanktis* TAC125: from the structure to the physiological functions. *Adv Microb Physiol* **63**, 329–89.
 12. Parrilli E, Giuliani M, Giordano D, Russo R, Marino G, Verde C & Tutino ML (2010) The role of a 2-on-2 haemoglobin in oxidative and nitrosative stress resistance of Antarctic *Pseudoalteromonas haloplanktis* TAC125. *Biochimie* **92**, 1003–1009.
 13. Howes BD, Giordano D, Boechi L, Russo R, Mucciacciaro S, Ciaccio C, Sinibaldi F, Fittipaldi M, Marti MA, Estrin DA, di Prisco G, Coletta M, Verde C & Smulevich G (2011) The peculiar heme pocket of the 2/2 hemoglobin of cold-adapted *Pseudoalteromonas haloplanktis* TAC125. *J Biol Inorg Chem* **16**, 299–311.
 14. Giordano D, Russo R, Ciaccio C, Howes BD, di Prisco G, Smulevich G, Coletta M & Verde C (2011) Ligand- and proton-linked conformational changes of the ferrous 2/2 hemoglobin of *Pseudoalteromonas haloplanktis* TAC125. *IUBMB Life* **63**, 566–573.
 15. Russo R, Giordano D, di Prisco G, Hui Bon Hoa G, Marden MC, Verde C & Kiger L (2013) Ligand-rebinding kinetics of 2/2 hemoglobin from the Antarctic bacterium *Pseudoalteromonas haloplanktis* TAC125. *Biochim Biophys Acta* **1834**, 1932–1938.
 16. Coppola D, Giordano D, Tinajero-Trejo M, di Prisco G, Ascenzi P, Poole RK & Verde C (2013) Antarctic bacterial hemoglobin and its role in the protection against nitrogen reactive species. *Biochim Biophys Acta* **1834**, 1923–1931.
 17. Laskowski RA, MacArthur MW, Moss DS & Thornton JM (1993) PROCHECK, a program to check the stereochemical quality of protein structure. *J Appl Crystallogr* **26**, 283–291.

- 1
2 18. Krissinel E & Henrick K (2005) Detection of Protein Assemblies in Crystals. In:
3
4 *Computational Life Science*, (Berthold MR, Glen RC, Diederichs K, Kohlbacher O & Fischer I
5 ed), pp. 163–174. Springer Berlin Heidelberg.
6
7
8
9 19. Nardini M, Pesce A, Milani M & Bolognesi M (2007) Protein fold and structure in the
10 truncated (2/2) globin family. *Gene* **398**, 2–11.
11
12
13 20. Milani M, Pesce A, Nardini M, Ouellet H, Ouellet Y, Dewilde S, Bocedi A, Ascenzi P,
14 Guertin M, Moens L, Friedman JM, Wittenberg JB & Bolognesi M (2005) Structural bases for
15 heme binding and diatomic ligand recognition in truncated hemoglobins. *J Inorg Biochemistry*
16 **99**, 97–109.
17
18
19
20
21
22 21. Milani M, Pesce A, Ouellet H, Guertin M & Bolognesi M (2003) Truncated
23 hemoglobins and nitric oxide action. *IUBMB Life* **55**, 623–627.
24
25
26
27 22. Egawa T & Yeh SR (2005) Structural and functional properties of hemoglobins from
28 unicellular organisms as revealed by resonance Raman spectroscopy. *J Inorg Biochem* **99**, 72–
29 96.
30
31
32
33 23. Das TK, Couture M, Lee HC, Peisach J, Rousseau DL, Wittenberg BA, Wittenberg JB
34 & Guertin M (1999) Identification of the ligands to the ferric heme of *Chlamydomonas*
35 chloroplast hemoglobin: evidence for ligation of tyrosine-63 (B10) to the heme. *Biochemistry*
36 **38**, 15360–15368.
37
38
39
40 24. Caillet-Saguy C, Turano P, Piccioli M, Lukat-Rodgers GS, Czjzek M, Guigliarelli B,
41 Izadi-Pruneyre N, Rodgers KR, Delepierre M & Lacroisey A (2008) Deciphering the structural
42 role of histidine 83 for heme binding in hemophore HasA. *J Biol Chem* **283**, 5960–5970.
43
44
45
46 25. Alontaga AY, Rodriguez JC, Schonbrunn E, Becker A, Funke T, Yukl ET, Hayashi T,
47 Stobaugh J, Moenne-Loccoz P & Rivera M (2009) Structural characterization of the
48 hemophore HasAp from *Pseudomonas aeruginosa*: NMR spectroscopy reveals protein-protein
49 interactions between Holo-HasAp and hemoglobin. *Biochemistry* **48**, 96–109.
50
51
52
53
54
55
56
57
58
59
60

- 1
2
3
4
5
6
7
8
9
10
11
12
13
14
15
16
17
18
19
20
21
22
23
24
25
26
27
28
29
30
31
32
33
34
35
36
37
38
39
40
41
42
43
44
45
46
47
48
49
50
51
52
53
54
55
56
57
58
59
60
26. Smulevich G, Miller MA, Kraut J & Spiro TG (1991) Conformational change and histidine control of heme chemistry in cytochrome c peroxidase: resonance Raman evidence from Leu-52 and Gly-181 mutants of cytochrome c peroxidase. *Biochemistry* **30**, 9546–9558.
27. Que L (1988) Metal-tyrosinate proteins. In: *Biological applications of Raman spectroscopy*, (Spiro TG, ed), pp. 491–521. Wiley, NY.
28. Nagai M, Yoneyama Y & Kitagawa T (1989) Characteristics in tyrosine coordinations of four hemoglobins M probed by resonance Raman spectroscopy. *Biochemistry* **28**, 2418–2422.
29. Aki Y, Nagai M, Nagai Y, Imai K, Aki M, Sato A, Kubo M, Nagatomo S & Kitagawa T (2010) Differences in coordination states of substituted tyrosine residues and quaternary structures among hemoglobin M probed by resonance Raman spectroscopy. *J Biol Inorg Chem* **15**, 147–158.
30. Sharma KD, Andersson LA, Loehr TM, Turner J & Goff HM (1989) Comparative spectral analysis of mammalian, fungal, and bacterial catalases. Resonance Raman evidence for iron-tyrosinate coordination. *J Biol Chem* **264**, 12772–12779.
31. Eakanukul S, Lukat-Rodgers GS, Sumithran S, Ghosh A, Rodgers KR, Dawson JH & Wilks A (2005) Characterization of the periplasmic heme-binding protein shut from the heme uptake system of *Shigella dysenteriae*. *Biochemistry* **44**, 13179–13191.
32. Nicoletti FP, Howes BD, Fittipaldi M, Fanali G, Fasano M, Ascenzi P & Smulevich G (2008) Ibuprofen induces an allosteric conformational transition in the heme complex of human serum albumin with significant effects on heme ligation. *J Am Chem Soc* **130**, 11677–11688.
33. Reeder BJ, Svistunenko DA & Wilson MT (2011) Lipid binding to cytoglobin leads to a change in haem co-ordination: a role for cytoglobin in lipid signalling of oxidative stress. *Biochemistry* **434**, 483–492.

- 1
2 34. Cerda-Colon JF, Silfa E & Lopez-Garriga J (1998) Unusual rocking freedom of the
3
4 heme in the hydrogen sulfide-binding hemoglobin from *Lucina pectinata*. *J Am Chem Soc* **120**,
5
6 9312–9317.
7
8
9 35. Kraus DW, Wittenberg JB, Lu JF & Peisach J (1990) Hemoglobins of the *Lucina*
10
11 *pectinata*/bacteria symbiosis. II. An electron paramagnetic resonance and optical spectral study
12
13 of the ferric proteins. *J Biol Chem* **265**, 16054–16059.
14
15
16 36. Feis A, Marzocchi MP, Paoli M & Smulevich G (1994) Spin state and axial ligand
17
18 bonding in the hydroxide complexes of metmyoglobin, methemoglobin, and horseradish
19
20 peroxidase at room and low temperatures. *Biochemistry* **33**, 4577–4583.
21
22
23 37. Mukai M, Savard PY, Ouellet H, Guertin M & Yeh SR (2002) Unique ligand-protein
24
25 interactions in a new truncated hemoglobin from *Mycobacterium tuberculosis*. *Biochemistry*
26
27 **41**, 3897–3905.
28
29
30 38. Nicoletti FP, Bustamante JP, Droghetti E, Howes BD, Fittipaldi M, Bonamore A,
31
32 Baiocco P, Feis A, Boffi A, Estrin DA & Smulevich G (2014) Interplay of the H-Bond
33
34 Donor–Acceptor Role of the Distal Residues in Hydroxyl Ligand Stabilization of *Thermobifida*
35
36 *fusca* Truncated Hemoglobin. *Biochemistry* **53**, 8021–8030.
37
38
39 39. Yeh SR, Couture M, Ouellet Y, Guertin M & Rousseau DL (2000) A cooperative
40
41 oxygen binding hemoglobin from *Mycobacterium tuberculosis*. Stabilization of heme ligands
42
43 by a distal tyrosine residue. *J Biol Chem* **275**, 1679–1684.
44
45
46 40. Couture M, Das TK, Savard P-Y, Ouellet Y, Wittenberg JB, Wittenberg BA, Rousseau
47
48 DL & Guertin M (2000) Structural investigations of the hemoglobin of the cyanobacterium
49
50 *Synechocystis* PCC6803 reveal a unique distal heme pocket. *Eur. J. Biochem.* **267**, 4770–4780.
51
52
53 41. Das TK, Franzen S, Pond A, Dawson JH & Rousseau DL (1999) Formation of a five-
54
55 coordinate hydroxide-bound heme in the His93Gly mutant of sperm whale myoglobin. *Inorg*
56
57 *Chem* **38**, 1952–1953.
58
59
60

- 1
2
3
4
5
6
7
8
9
10
11
12
13
14
15
16
17
18
19
20
21
22
23
24
25
26
27
28
29
30
31
32
33
34
35
36
37
38
39
40
41
42
43
44
45
46
47
48
49
50
51
52
53
54
55
56
57
58
59
60
42. Das TK, Boffi A, Chiancone E & Rousseau DL (1999) Hydroxide rather than histidine is coordinated to the heme in five-coordinate ferric *Scapharca inaequivalvis* hemoglobin. *J Biol Chem* **274**, 2916–2919.
43. Howes BD, Rodriguez-Lopez JN, Smith AT & Smulevich G (1997) Mutation of distal residues of horseradish peroxidase: influence on substrate binding and cavity properties. *Biochemistry* **36**, 1532–1543.
44. Boechi L, Martí MA, Milani M, Bolognesi M, Luque FJ & Estrin DA (2008) Structural determinants of ligand migration in *Mycobacterium tuberculosis* truncated hemoglobin O. *Proteins* **73**, 372–379.
45. Boechi L, Mañez PA, Luque FJ, Marti MA & Estrin DA (2010) Unraveling the molecular basis for ligand binding in truncated hemoglobins: the trHbO *Bacillus subtilis* case. *Proteins* **78(4)**, 962–70.
46. Droghetti E, Nicoletti FP, Bonamore A, Boechi L, Arroyo Manez P, Estrin DA, Boffi A, Smulevich G & Feis A (2010) Heme pocket structural properties of a bacterial truncated hemoglobin from *Thermobifida fusca*. *Biochemistry* **49**, 10394–10402.
47. Feis A, Lapini B, Catacchio B, Brogioni S, Foggi P, Chiancone E, Boffi A & Smulevich G (2008) Unusually strong H-bonding to the heme ligand and fast geminate recombination dynamics of the carbon monoxide complex of *Bacillus subtilis* truncated hemoglobin. *Biochemistry* **47**, 902–910.
48. Chen Z, Cheng CH, Zhang J, Cao L, Chen L, Zhou L, Jin Y, Ye H, Deng C, Dai Z, Xu Q, Hu P, Sun S, Shen Y & Chen L (2008) Transcriptomic and genomic evolution under constant cold in Antarctic notothenioid fish. *Proc Natl Acad Sci USA* **105**, 12944–12949.
49. Rodrigues DF & Tiedje JM (2008) Coping with our cold planet. *Appl Environ Microbiol* **74**, 1677–1686.
50. D'Amico S, Collins T, Marx JC, Feller G & Gerday C (2006) Psychrophilic microorganisms: challenges for life. *EMBO Rep* **7**, 385–389.

- 1
2 51. Siddiqui KS & Cavicchioli R (2006) Cold-adapted enzymes. *Annu Rev Biochem* **75**,
3
4 403–433.
5
6
7 52. Riccio A, Vitagliano L, di Prisco G, Zagari A & Mazzarella L (2002) The crystal
8
9 structure of a tetrameric hemoglobin in a partial hemichrome state. *Proc Natl Acad Sci USA* **99**,
10
11 9801–9806.
12
13
14 53. Giordano D, Boechi L, Vergara A, Martí MA, Samuni U, Dantsker D, Grassi L, Estrin
15
16 DA, Friedman JM, Mazzarella L, di Prisco G & Verde C (2009) The hemoglobins of the sub-
17
18 Antarctic fish *Cottoperca gobio*, a phyletically basal species--oxygen-binding equilibria,
19
20 kinetics and molecular dynamics. *FEBS J* **276**, 2266–2277.
21
22
23 54. Boron I, Russo R, Boechi L, Cheng CH, di Prisco G, Estrin DA, Verde C & Nadra AD
24
25 (2011) Structure and dynamics of Antarctic fish neuroglobin assessed by computer simulations.
26
27 *IUBMB Life* **63**, 206–213.
28
29
30 55. Balsamo A, Sannino F, Merlino A, Parrilli E, Tutino ML, Mazzarella L & Vergara A
31
32 (2012) Role of the tertiary and quaternary structure in the formation of bis-histidyl adducts in
33
34 cold-adapted hemoglobins. *Biochimie* **94**, 953–960.
35
36
37 56. Smulevich G, Wang Y, Mauro JM, Wang JM, Fishel LA, Kraut J & Spiro TG (1990)
38
39 Single-crystal resonance Raman spectroscopy of site-directed mutants of cytochrome c
40
41 peroxidase. *Biochemistry* **29**, 7174-7180.
42
43
44 57. Indiani C, Santoni E, Becucci M, Boffi A, Fukuyama F & Smulevich G (2003) New
45
46 insight into the peroxidase-hydroxamic acid interaction revealed by the combination of
47
48 spectroscopic and crystallographic studies. *Biochemistry* **42**, 14066-14074.
49
50
51 58. Sezer M, Santos A, Kielb P, Pinto T, Martins LO & Todorovic S (2013) Distinct
52
53 structural and redox properties of the heme active site in bacterial dye decolorizing peroxidase-
54
55 type peroxidases from two subfamilies: resonance Raman and electrochemical study.
56
57 *Biochemistry* **52**, 3074–3084.
58
59
60

- 1
2
3
4
5
6
7
8
9
10
11
12
13
14
15
16
17
18
19
20
21
22
23
24
25
26
27
28
29
30
31
32
33
34
35
36
37
38
39
40
41
42
43
44
45
46
47
48
49
50
51
52
53
54
55
56
57
58
59
60
59. Ouellet H, Juszczak L, Dantsker D, Samuni U, Ouellet YH, Savard PY, Wittenberg JB, Wittenberg BA, Friedman JM & Guertin M (2003) Reactions of *Mycobacterium tuberculosis* truncated hemoglobin O with ligands reveal a novel ligand-inclusive hydrogen bond network. *Biochemistry* **42**, 5764–5774.
60. Marcelli A, Abbruzzetti S, Bustamante JP, Feis A, Bonamore A, Boffi A, Gellini C, Salvi PR, Estrin DA, Bruno S, Viappiani C & Foggi P (2012) Following ligand migration pathways from picoseconds to milliseconds in type II truncated hemoglobin from *Thermobifida fusca*. *PloS One* **7**, e39884.
61. Leslie AGM (2003) *MOSFLM User Guide, Mosflm Version 6.2.3*, MRC Laboratory of Molecular Biology, Cambridge, UK.
62. Evans P (2006) Scaling and assessment of data quality. *Acta Crystallogr D Biol Crystallogr* **62**, 72–82.
63. Claude JB, Suhre K, Notredame C, Claverie JM & Abergel C (2004) CaspR: a web-server for automated molecular replacement using homology modelling. *Nucleic Acids Res* **32**, 606–609.
64. Emsley P & Cowtan K (2004) Coot: model-building tools for molecular graphics. *Acta Crystallogr D Biol Crystallogr* **60**, 2126–2132.
65. Murshudov GN, Vagin AA & Dodson EJ (1997) Refinement of macromolecular structures by the maximum-likelihood method. *Acta Crystallogr D Biol Crystallogr* **53**, 240–255.
66. Laskowski RA (1995) SURFNET: a program for visualizing molecular surfaces, cavities, and intermolecular interactions. *J Mol Graph* **13**, 323–330.
67. Pearlman DA, Case DA, Caldwell JW, Ross WS, Cheatham III TE, DeBolt S, Ferguson D, Seibel G & Kollman P (1995) AMBER, a package of computer programs for applying molecular mechanics, normal mode analysis, molecular dynamics and free energy calculations

1
2 to simulate the structural and energetic properties of molecules. *Comput Phys Commun* **91**, 1–
3
4 41.

5
6 68. Ryckaert JP, Ciccotti G & Berendsen HJC (1977) Numerical integration of the cartesian
7
8 equations of motion of a system with constraints: molecular dynamics of n-alkanes. *J Comput*
9
10 *Phys* **23**, 327–341.

11
12
13 69. Cohen J, Olsen KW & Schulten K (2008) Finding gas migration pathways in proteins
14
15 using implicit ligand sampling. *Methods Enzymol* **437**, 439–457.

16
17
18 70. Forti F, Boechi L, Estrin DA & Marti MA (2011) Comparing and combining implicit
19
20 ligand sampling with multiple steered molecular dynamics to study ligand migration processes
21
22 in heme proteins. *J Comput Chem* **32(10)**, 2219–2231.
23
24
25
26
27
28
29
30
31
32
33
34
35
36
37
38
39
40
41
42
43
44
45
46
47
48
49
50
51
52
53
54
55
56
57
58
59
60

Supporting information

Table S1. Comparison of the EPR spectral parameters of various LS hemoproteins.

Table S2. Vibrational assignment and RR frequencies (cm^{-1}) of *Ph-2/2HbO* at pH 7.6 in the high-frequency region, based on the curve fitting analysis of the RR spectra in Fig. S2.

Table S3. Vibrational assignment and RR frequencies (cm^{-1}) of *Ph-2/2HbO* at pH 7.6 in the low-frequency region, based on the curve fitting analysis of the RR spectra in Fig. S3.

Table S4. Vibrational assignment and RR frequencies (cm^{-1}) of *Ph-2/2HbO* at pH 10.7 in the high-frequency region, based on the curve fitting analysis of the RR spectra in Fig. S4.

Table S5. Vibrational assignment and RR frequencies (cm^{-1}) of *Ph-2/2HbO* at pH 10.7 in the low-frequency region, based on the curve fitting analysis of the RR spectra in Fig. S5.

Fig. S1. The quaternary assembly of two *Ph-2/2HbO* chains observed in the crystal asymmetric unit.

Fig. S2. Curve fittings of the *Ph-2/2HbO* RR spectra in the high-frequency region shown in Fig. 5 obtained with excitation at 413.1, 496.5 and 514.5 nm (pH 7.6).

Fig. S3. Curve fittings of the *Ph-2/2HbO* RR spectra in the low-frequency region shown in Figure 5 obtained with excitation at 413.1, 496.5 and 514.5 nm (pH 7.6).

Fig. S4. Curve fittings of the *Ph-2/2HbO* RR spectra in the high-frequency region shown in Figure 5 obtained with excitation at 514.5 nm (pH 10.7).

Fig. S5. Curve fittings of the *Ph-2/2HbO* RR spectra in the low-frequency region shown in Figure 5 obtained with excitation at 514.5 nm (pH 10.7).

Fig. S6. Comparison of the RR spectra of *Ph-2/2HbO* at pH 7.6 and 10.7 at 298 K and 12 K.

Fig. S7. Low-frequency region RR spectra of alkaline *Ph-2/2HbO* at 298 K, in H_2O , D_2O , and H_2^{18}O buffered solutions.

Fig. S8. Schematic representation of the X-ray distal heme cavity of *Ph-2/2HbO* (light orange) and the average structure obtained by MD simulations in the absence of a distal heme ligand.

1
2 **Fig. S9.** Time evolution of Fe-O_{Tyr(42)}B10 distances for *Ph*-2/2HbO (black), *Mt*-2/2HbO (red)
3
4 and *Tf*-2/2HbO (green).

5
6 **Fig. S10.** RMSF (Å) for backbone atoms in WT deoxy forms of *Ph*-2/2HbO (black), *Mt*-
7
8 2/2HbO (green) and *Tf*-2/2HbO (red) at 300K. *Ph*-2/2HbO shows major fluctuations in the EF
9
10 loop (residues 79 to 83).

11
12 **Fig. S11.** Time evolution (ns) of RMSD (Å) for the backbone atoms in the deoxy form of *Ph*-
13
14 2/2HbO (black), and for OH⁻ heme liganded ferric species (green).

15
16 **Fig. S12.** Time evolution (ns) of RMSD (Å) for backbone atoms of *Ph*-2/2HbO hosting CO
17
18 (blue) and O₂ (red) as ligands bound to the heme.
19
20
21
22
23
24
25
26
27
28
29
30
31
32
33
34
35
36
37
38
39
40
41
42
43
44
45
46
47
48
49
50
51
52
53
54
55
56
57
58
59
60

Table 1. Data collection and crystallographic refinement statistics for *Ph-2/2HbO*.

Data collection	
Space group	$P2_12_12_1$
Cell dimensions:	
a, b, c (Å)	42.9, 72.3, 88.3
α, β, γ (°)	90, 90, 90
Wavelength (Å)	0.979
Resolution (Å)	72.25-2.21 (2.33-2.21) ^a
No. reflections	63042
Unique reflections	14322
R_{merge}^b	0.102 (0.451)
$I/\sigma(I)$	8.7 (3.1)
Completeness (%)	99.5 (99.7)
Multiplicity	4.4 (4.6)
Refinement	
Resolution (Å)	44.15-2.21
$R_{\text{factor}}/R_{\text{free}}$ (%)	18.3/24.6
No. of residues/protein atoms	248 (2x124, from residue 22 to 145)/2132
No. of heme groups	2
No. of water molecules	62
B-factors (Å ²):	
Protein	40.1
Heme group	31.3
Water molecules	38.3
RMSD from ideality:	
bond lengths (Å)	0.015
bond angles (°)	1.7
Ramachandran plot ^c :	
most favored regions (%)	94.8
additional allowed regions (%)	5.2

^aValues in parentheses are for highest-resolution shell

^b $R_{\text{merge}} = \sum_h \sum_i |I_{hi} - \langle I_h \rangle| / \sum_h \sum_i I_{hi}$.

^cData produced using the program PROCHECK [17]

Table 2. Tyrosinate vibrational bands (cm^{-1}) of ferric-heme proteins with tyrosinate ligation.

Protein	Spin state	$\nu_{\text{Tyr}}(\text{C}=\text{C})$	$\nu_{\text{Tyr}}(\text{C}=\text{C})$	$\nu_{\text{Tyr}}(\text{C}-\text{O})$	$\nu(\text{Fe}-\text{O}_{\text{Tyr}})$	Reference
<i>Ph-2/2HbO</i>	6cLS	*	1509	1312	590	This work
<i>Chlamydomonas</i> Hb	6cLS	1595	1500	1308	502	[23]
Hb M Saskatoon	6cHS	1607	1504	1300	581/598	[28,29]
Hb M Boston	5cHS	1603	1504	1279	603	[28]
Hb M Iwate	5cHS	1607	1504	1308	588	[28]
Hb M Hyde Park	5cHS	1609	1502	1300	588	[28]
<i>Aspergillus niger</i> catalase	5cHS	1615	-	1245	-	[30]
<i>Shigella dysenteriae</i> ShuT	5cHS	1601	1502	1301/1265	613	[31]

* This band is not observed, as it overlaps those at 1602 cm^{-1} and 1609 cm^{-1} (ν_{37} and ν_{10}) determined by a curve-fitting analysis (Fig. S2, Table S2).

Table 3. RR frequencies (cm^{-1}) of the $\nu(\text{Fe-OH})$ modes of various heme proteins at alkaline pH. The observed isotopic shifts are in parentheses.

Protein	6cHS (D_2O , H_2^{18}O)	6cLS (D_2O , H_2^{18}O)	5cHS (D_2O , H_2^{18}O)	Reference
<i>Ph-2/2HbO</i>		528 (+6,-18)	568 (-14,-19)	This work
<i>Mt-2/2HbO</i>	446 (nr, 22)	533 (nr, -30)		[37]
<i>Tf-2/2HbO</i>		485 (+4, -14)		[38]
<i>Mt-2/2HbN</i>	454 (nr,-31)	561 (nr,-28)		[39]
<i>Synechocystis 2/2HbS</i>			573 (nr, -24)	[40]
Mb (horse heart)	491 (-14,-23)	550 (-12,-25)		[36]
Hb (human)	492 (-13,nr)	553 (-9,nr)		[36]
HRPC		516 (+6,-19)		[36]
H93G Mb (sperm whale)			575 (-13,-24)	[41]
<i>Scapharca inaequalvis</i> Hb			578 (nr,-25)	[42]

Figure legends

Fig. 1. Ribbon representation of the three-dimensional fold of *Ph-2/2HbO*. The heme group is in red and the helices are labelled; proximal His(96)F8 is shown as stick model. Helix A is just a one-turn helical segment following the N terminus. Note that the presence of the additional helix Φ , between helices E and F, is specific for TrHbIIs.

Fig. 2. Structure-based sequence alignment of *Ph-2/2HbO* with members of the TrHbII family whose crystal structures are available. Helical regions are shaded in grey and the TrHbII-specific helix Φ is indicated; residues (B10, CD1 and G8) specific for TrHbIIs are in yellow; HisF8, conserved in the globin superfamily, is in magenta; the Gly-Gly motifs are in cyan. The main differences (in sequence and structure) are located in the N- and C-terminal regions, and in the BC, CE, and GH loops.

Fig. 3. (A): Location of distal and exposed cavities throughout the protein matrix in *Ph-2/2HbO*, separated by the Ile(65)E7 side chain. The heme group is in red and the cavity system is highlighted as a pink mesh. The residues defining an alternative access to the heme distal site are labelled. (B): Heme pocket structure in *Ph-2/2HbO*. The Figure shows some of the residues involved in stabilization of the heme through Fe coordination, i.e. His(96)F8, salt bridges and/or H bonds with Arg(64)E6 and Arg(95)F7. The Figure also displays the protein environment surrounding the heme-Fe atom coordinated water molecule (W32, shown as a magenta sphere) in the A subunit. The side chains of residues involved in interactions with the coordinated water molecule are shown and labelled. The additional water molecule W13 (magenta sphere), that is an integral part of the distal site H-bonded network stabilising the heme ligand, is also shown.

Fig. 4. Ferric *Ph-2/2HbO* at pH 7.6 and 10.9. (A): UV-vis absorption (continuous line) and D2 (dotted line) spectra. The visible region has been expanded five-fold. Spectra have been shifted along the ordinate axis to allow better visualization. (B): X-band EPR spectrum. Spectra were recorded at 5 K, 9.39-GHz microwave frequency, 1-mW microwave power and 10 G modulation amplitude. (C, D): RR spectra were recorded with the 413.1-nm excitation wavelength. Experimental conditions: 15-mW laser power at the sample, 1-cm⁻¹ spectral resolution, average of twelve spectra (C) and four spectra (D) with 600-s integration time. The intensities are normalized to those of the ν_7 band (678 cm⁻¹) (C) and the ν_4 band (1371 cm⁻¹) (D).

1
2
3
4 **Fig. 5.** RR spectra of *Ph-2/2HbO* at pH 7.6 and 10.7 at the excitation wavelengths shown.
5 Experimental conditions: pH 7.6: 413.1 nm, see Fig. 4; 496.5 nm 70-mW laser power at the
6 sample, 2.4-cm⁻¹ spectral resolution, average of 9 spectra with 600-s integration time (high
7 frequency), average of 36 spectra with 600-s integration time (low frequency); 514.5 nm, 140-
8 mW laser power at the sample, 2.2-cm⁻¹ spectral resolution, average of 4 spectra with 600-s
9 integration time (high frequency); average of 18 spectra with 600-s integration time (low
10 frequency); pH 10.7: 514.5 nm, average of 15 spectra with 600-s integration time (high
11 frequency); average of 36 spectra with 600-s integration time (low frequency). The tyrosinate
12 modes are in blue. The asterisks indicate bands due to the alkaline buffer CAPS. The $\delta(\text{H-O-H})$
13 water bending mode has been subtracted from the spectra taken in the visible region.
14
15
16
17
18
19
20
21
22

23 **Fig. 6.** (A and C): low-frequency region RR spectra of alkaline *Ph-2/2HbO*, at 12 and 298 K,
24 respectively, obtained in H₂O, D₂O, and H₂¹⁸O buffered solutions. (B and D): difference
25 spectra, H₂O-D₂O, D₂O-H₂¹⁸O, and H₂O-H₂¹⁸O, at 12 and 298 K, respectively. Experimental
26 conditions as in Figure 4; 298 K: average of 12 spectra with 600 s integration time (H₂O, D₂O),
27 average of 4 spectra with 600 s integration time (H₂¹⁸O); 12 K: average of 12 spectra with 600 s
28 integration time.
29
30
31
32
33
34

35 **Fig. 7.** RR spectra of ferric *Ph-2/2HbO* at pH 7.6 (blue), 8.5 (magenta) and 10.9 (black).
36 Experimental conditions as in Fig. 4. Average of twelve spectra (A) and four spectra (B) with
37 600-s integration time. The intensities are normalized to those of the ν_7 band (678 cm⁻¹) (A)
38 and of the ν_4 band (1371 cm⁻¹) (B). The red arrows indicate the changes in relative intensity or
39 frequency upon raising pH.
40
41
42
43
44
45

46 **Figure 8** Schematic representation of the distal heme cavity of *Ph-2/2HbO* with CO (A) and O₂
47 (B) ligands stabilized by H-bonds. Time evolution of X-N_{TrpG8} (black) and X-O_{TyrB10} (red)
48 distances showing H-bond network interactions during the timescale of simulation for X=CO
49 (C) and X=O₂ (D) are also shown. Distances are in Å.
50
51
52
53
54

55 **Figure 9** Schematic representation of the heme distal pocket, the open E7 tunnel, and the cavity
56 system of *Ph-2/2HbO* along the MD simulation (violet surface), superimposed on the crystal
57 structure (light orange atoms and yellow cavity).
58
59
60

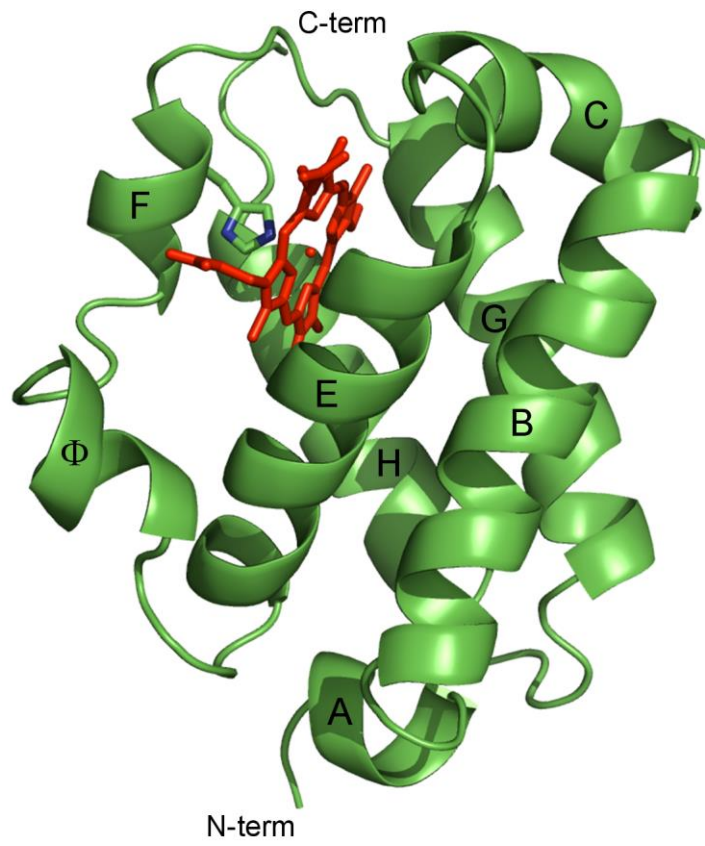


Fig. 1

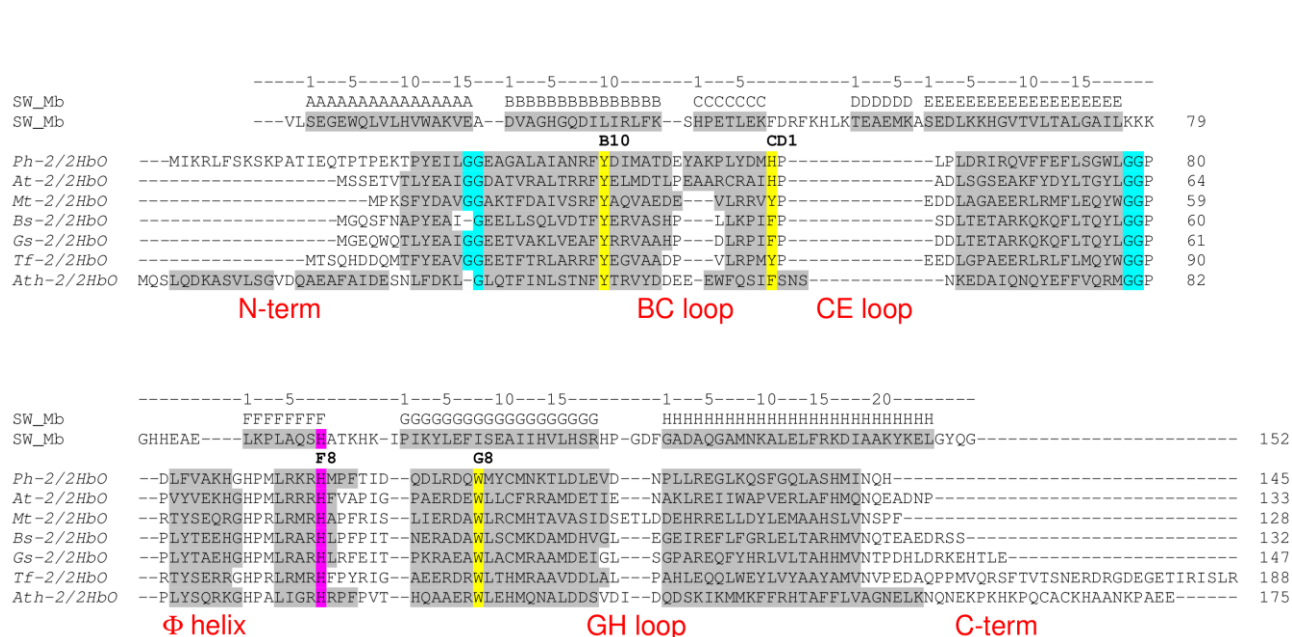
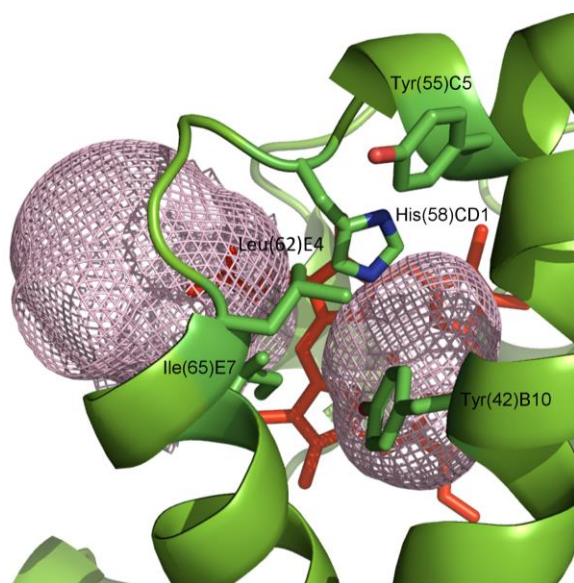


Fig. 2

A



B

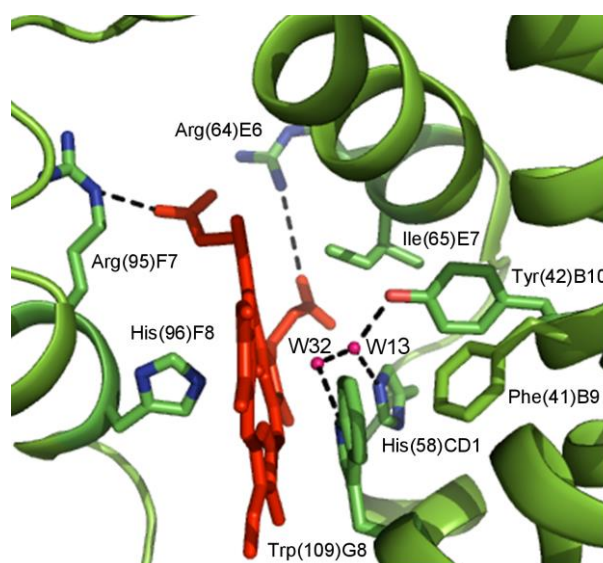


Fig. 3

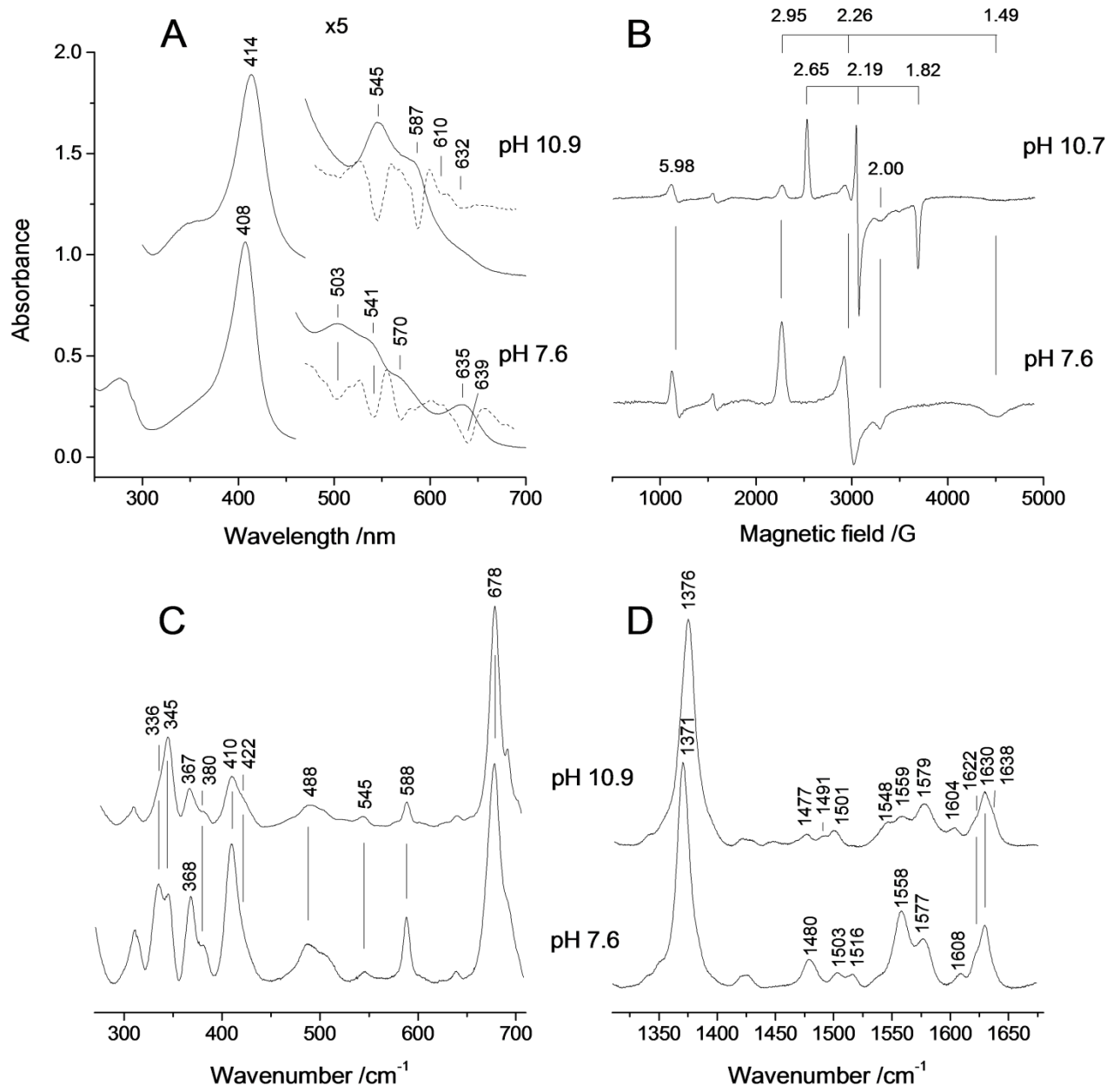


Fig. 4

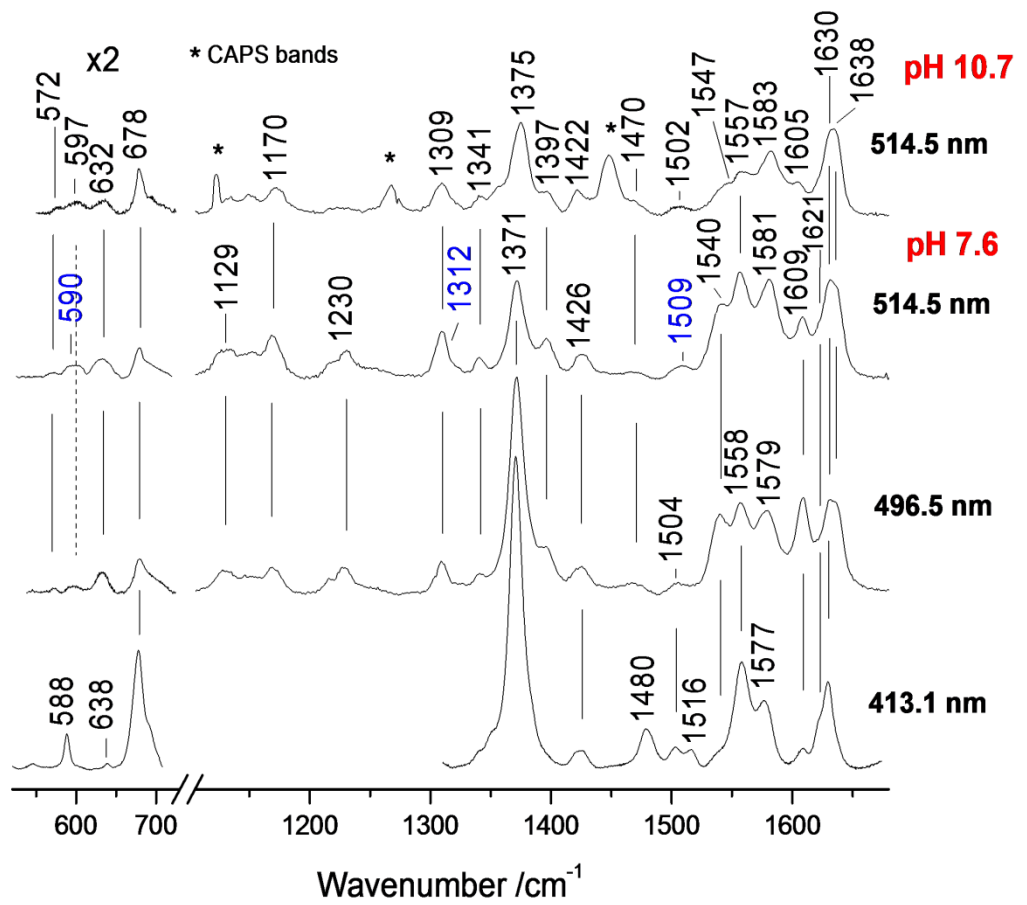


Fig. 5

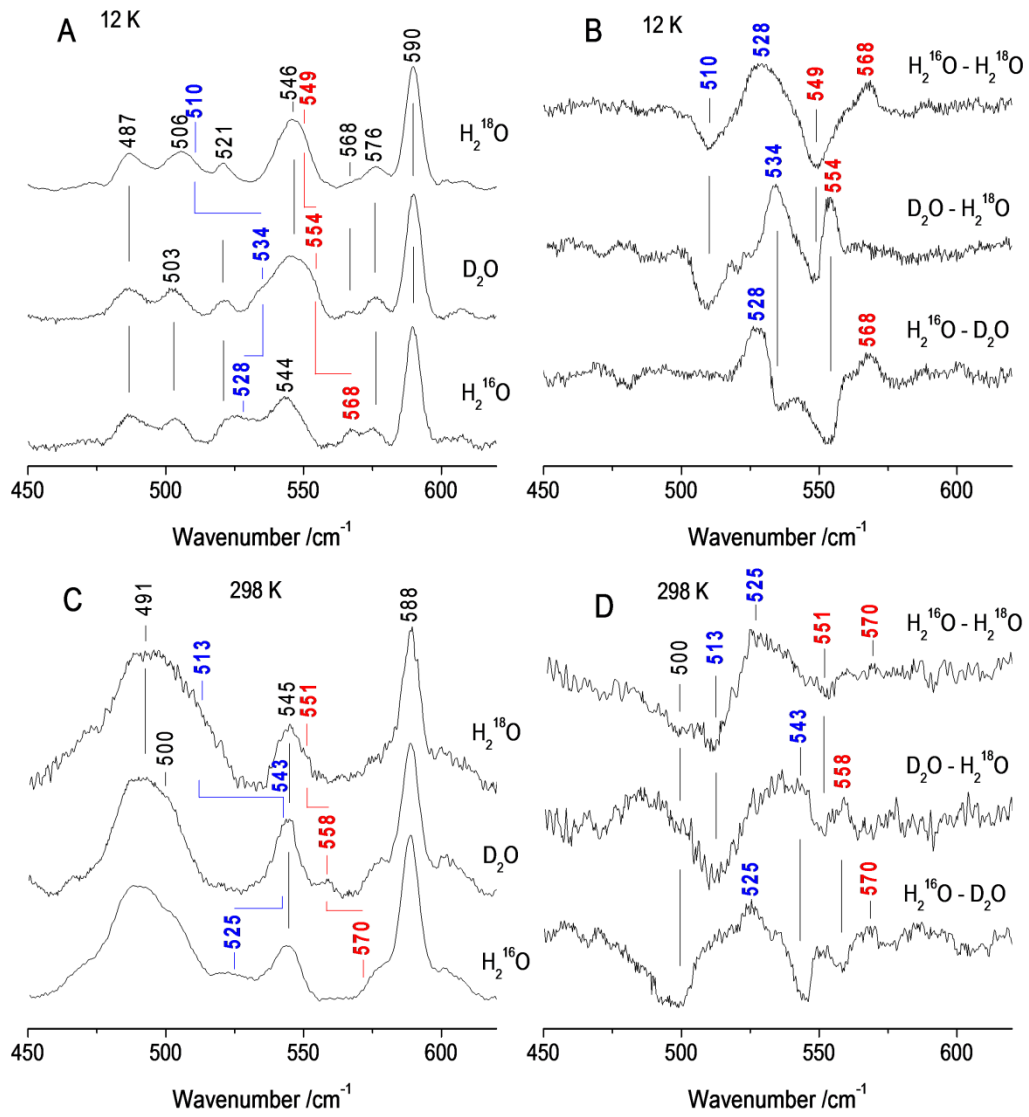


Fig. 6

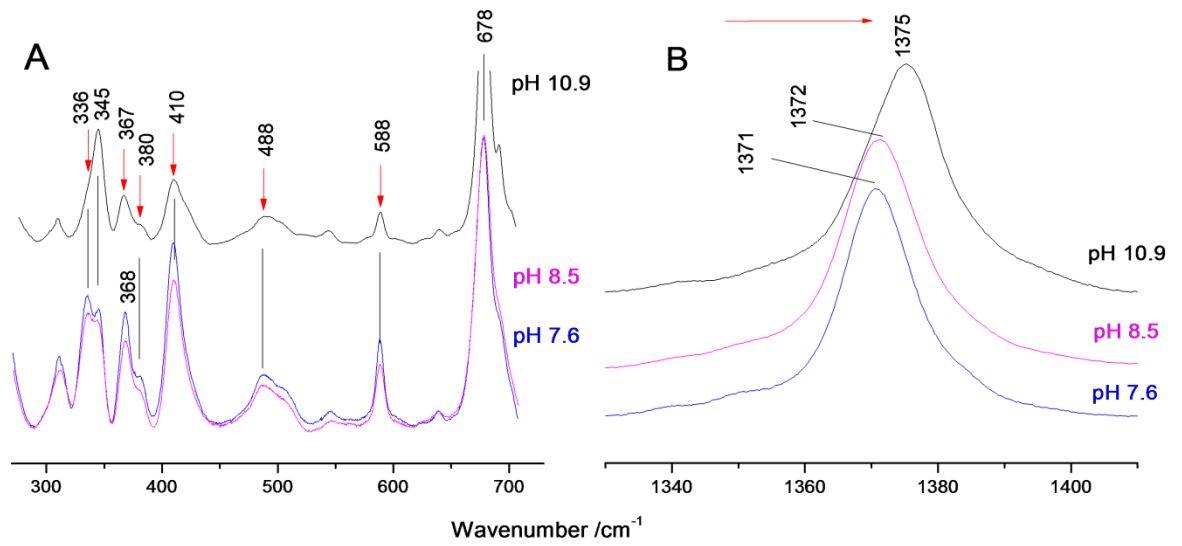


Fig. 7

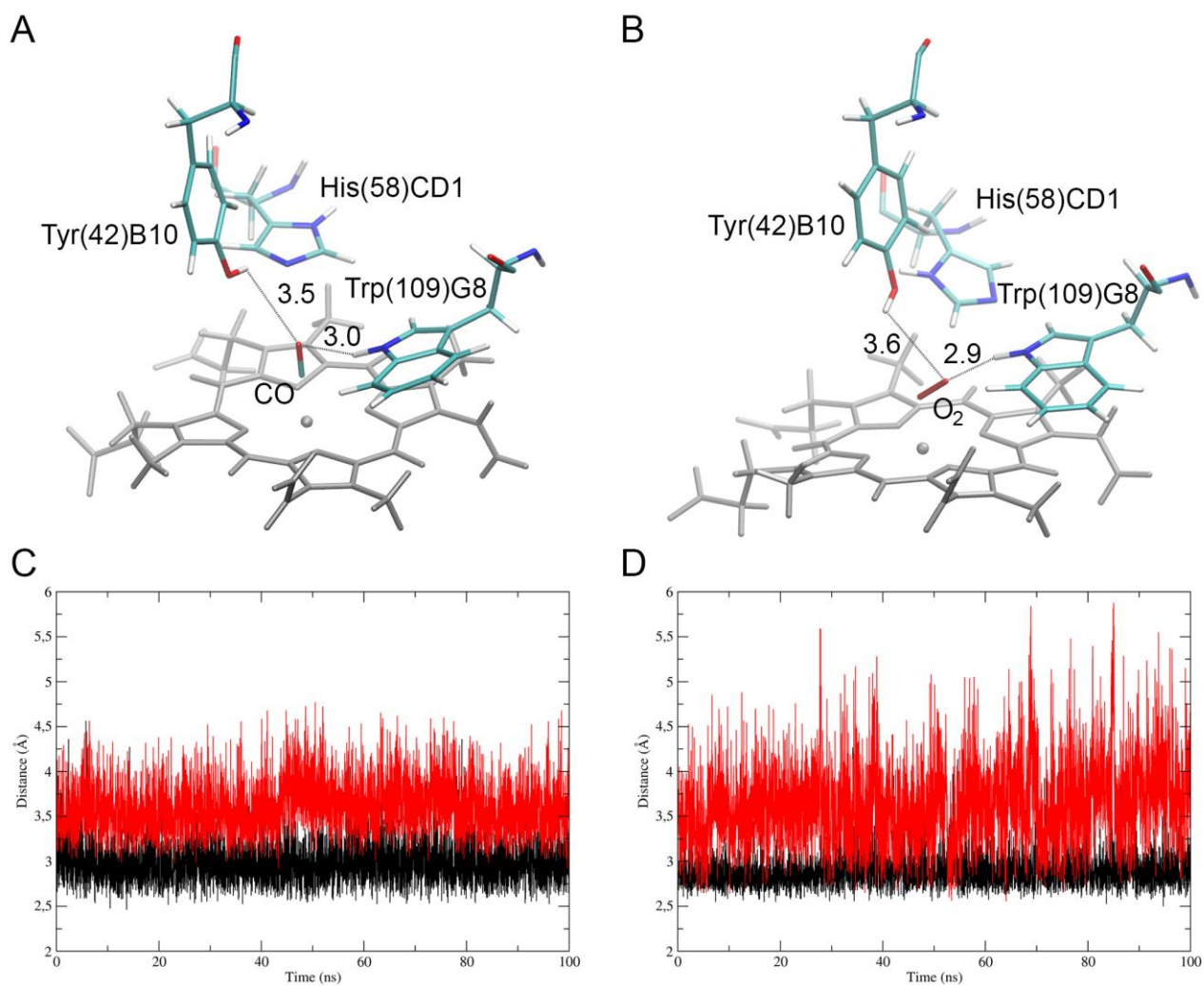
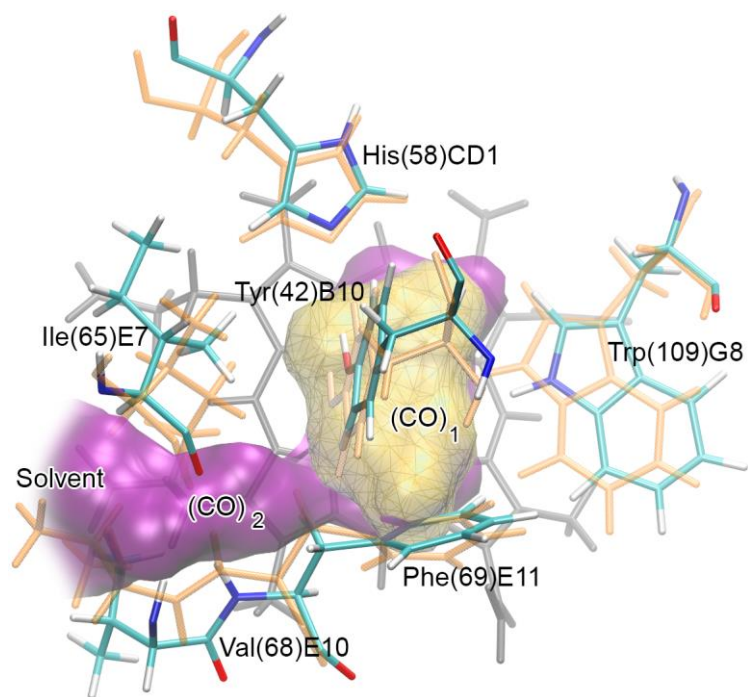


Fig. 8

**Fig. 9**